JGR Oceans

RESEARCH ARTICLE
10.1029/2021JC018369

The Effects of Light Intensity and Flow Speed on Biogeochemical Variability Within a Fringing Coral Reef in Onna-Son, Okinawa, Japan

M. S. Rintoul[1], T. A. Courtney[1,2], J. L. Dohner[1], S. N. Giddings[1], S. A. H. Kekuewa[1], S. Mitarai[3], S. G. Monismith[4], A. K. Pezner[1], and A. J. Andersson[1]

[1]Scripps Institution of Oceanography, University of California San Diego, La Jolla, CA, USA, [2]Department of Marine Sciences, University of Puerto Rico at Mayagüez, Mayagüez, Puerto Rico, [3]Marine Biophysics Unit, Okinawa Institute of Science and Technology, Okinawa, Japan, [4]Department of Civil and Environmental Engineering, Stanford University, Stanford, CA, USA

Key Points:

- Flow speed and light intensity explained 25%–74% of daily and 7%–75% of nightly pH and oxygen variability across different reef habitats
- Circulation of the Onna-son coral reef system was driven by waves, but modulated by tides, and was highly consistent
- Constraining coral reef circulation and light intensity will allow us to better predict future biogeochemical variability on coral reefs

Supporting Information:

Supporting Information may be found in the online version of this article.

Correspondence to:

M. S. Rintoul,
msrintou@ucsd.edu

Citation:

Rintoul, M. S., Courtney, T. A., Dohner, J. L., Giddings, S. N., Kekuewa, S. A. H., Mitarai, S., et al. (2022). The effects of light intensity and flow speed on biogeochemical variability within a fringing coral reef in Onna-son, Okinawa, Japan. *Journal of Geophysical Research: Oceans*, *127*, e2021JC018369. https://doi.org/10.1029/2021JC018369

Received 21 DEC 2021
Accepted 16 NOV 2022

Abstract Global warming and ocean acidification are driving declines in seawater dissolved oxygen (DO) concentrations and pH. Predicting how these changes will affect shallow, near-shore environments such as coral reefs is challenging due to their high natural biogeochemical variability present over both spatial (m to km) and temporal (diel to seasonal) scales. To make predictions, we must understand the drivers of this variability. The impact of metabolic processes on coral reef biogeochemical variability has been the subject of significant research effort, however, physical factors, including flow speed and light intensity, have received less attention. Here, we measured seawater flow, photosynthetically active radiation (PAR), pH, and DO at three reef habitats (reef flat, lagoon, and outflow channel) in a fringing coral reef system in Okinawa, Japan for 3 weeks in October 2019. During the study, pH ranged from 7.86 to 8.37 units while DO varied from 127 to 369 μmol/kg. Circulation was primarily wave-driven with mean flow speeds ranging from 14 to 26 cm/s. Flow direction became increasingly consistent at higher flow speeds and traced benthic striations visible in satellite imagery. Multiple linear regression models of daytime changes in pH and DO versus daily mean flow speed and PAR described 25%–74% of the observed variability across all sites while at night, flow speed alone accounted for 7%–75% of the observed variability. These results demonstrate PAR, water flow speed, and the path water takes play important roles in controlling biogeochemical variability within coral reefs and must be considered when assessing their vulnerability to both local and global environmental change.

Plain Language Summary Climate change is causing the ocean to lose oxygen and become more acidic. These changes will likely impact coral reefs but predicting how and when is challenging because coral reefs naturally experience large variations in oxygen and seawater acidity over both space and time. To predict how global changes will impact coral reefs, we must understand the drivers of this natural variability. Past research efforts have explored how much of this variability is caused by biological factors, but fewer efforts have investigated the influence of physical factors such as seawater flow speed and light intensity. In this study, we measured flow speed, light intensity, oxygen concentration, and seawater acid-base balance at three different habitats on a coral reef for 3 weeks in Okinawa, Japan. Using statistical models, we determined that daily variations in mean flow speed and light intensity accounted for 25%–74% of the variability during the day, and flow speed alone accounted for 7%–75% of the nighttime variability. These results show that flow speed and light intensity play important roles in controlling coral reef oxygen and pH variability and must be considered when assessing how climate change and future changes in seawater chemistry will impact coral reefs.

1. Introduction

Anthropogenic climate change is driving major changes in the world's oceans, including ocean warming (Domingues et al., 2008; Durack et al., 2018; Levitus et al., 2005), deoxygenation (Breitburg et al., 2018; Keeling et al., 2009), and acidification (Doney et al., 2009, 2020; Kleypas et al., 1999; Kwiatkowski & Orr, 2018). These changes pose serious threats to marine organisms and ecosystems (Andersson & Gledhill, 2013; Eyre et al., 2018; Hoegh-Guldberg et al., 2007; Hughes et al., 2003) by altering the roles, functions, and biogeochemical cycles of marine ecosystems (e.g., Guan et al., 2020; Hughes et al., 2017; Smale, 2020). Coral reefs may be particularly susceptible to these changes as evidenced by recent declines in global coral cover (Bruno & Selig, 2007; Gardner

et al., 2003; Jackson et al., 2014). Anomalously high seawater temperatures have driven recent global mass coral bleaching events and continued warming will increase the frequency and intensity of these events (Hughes et al., 2017; van Hooidonk et al., 2016). The incidence of coral disease and associated mortality are also likely to increase under warming (Glynn & Manzello, 2015; Ruiz-Moreno et al., 2012; van Hooidonk et al., 2013). Additionally, ocean warming decreases seawater oxygen concentrations and increases biological oxygen demand, potentially increasing the frequency and duration of hypoxic events that have been linked to mortality of reef organisms ranging from cryptic infauna to corals and fish (Altieri et al., 2017; Hobbs & McDonald, 2010; Kealoha et al., 2020; Raj et al., 2020). This problem is likely to be exacerbated in regions experiencing increased eutrophication (Altieri et al., 2017; Diaz & Rosenberg, 2008). While projected levels of acidification alone are unlikely to be lethal to most reef organisms, acidification will interact synergistically with warming and hypoxia to decrease the overall fitness of reef organisms (Anthony et al., 2008; Dove et al., 2013, 2020), reduce calcification rates (Albright et al., 2018; Guo et al., 2020), increase $CaCO_3$ dissolution and bioerosion rates (Albright et al., 2018; Cyronak et al., 2013; Eyre et al., 2018), and may contribute to decreasing reef biodiversity (Fabricius et al., 2011). It is highly likely that future warming, deoxygenation, and ocean acidification will alter the role and function of coral reefs and change their capacity to provide essential ecosystem services.

While it is certain that future climate change will affect coral reefs, predicting how different coral reefs and reef habitats will be affected under global and regional climate change scenarios is challenging owing to the large spatiotemporal variability in physico-biogeochemical parameters present in coral reef environments (e.g., Cyronak et al., 2020; Koweek et al., 2015; Smith et al., 2013). For example, contemporaneous seawater temperatures may vary by over 10°C between forereef and back reef environments depending on properties such as depth, reef geomorphology, flow rates, and residence times (DeCarlo et al., 2017; Guadayol et al., 2014; Lee et al., 2020; Reid et al., 2020; Safaie et al., 2018; Wyatt et al., 2020). Similarly, large spatial gradients in seawater pH and dissolved oxygen (DO) may be created by coral reef metabolic processes. The modification of seawater by reef metabolism is enhanced in areas of high biomass to seawater volume ratios (i.e., shallow depth) and as a function of increasing residence time (Cyronak et al., 2020; Kekuewa et al., 2021). Furthermore, reef seawater pH and DO concentrations may vary strongly over a diel cycle, with some reefs experiencing values that exceed the full range of changes anticipated for the open ocean under global climate change by the end of the century (Guadayol et al., 2014; Shaw et al., 2012). Similarly, seasonal and interannual variability in pH and DO concentrations largely exceeds changes attributable to climate change (Gattuso et al., 1993; Guadayol et al., 2014; Price et al., 2012). The large spatiotemporal variability present on coral reefs necessitates a nuanced approach to predict how reefs will be affected by future climate change, as physico-biogeochemical differences between and within different coral reef systems may alter their sensitivity and susceptibility to future conditions. Quantifying and understanding the drivers of these physico-biogeochemical differences will be critical for determining the vulnerability of certain reefs and reef habitats to climate change and for guiding management efforts (Darling et al., 2019; McClanahan et al., 2012).

Biogeochemical variability on coral reefs is influenced by both biological and physical factors. The dominant biogeochemical processes that alter reef seawater biogeochemistry include photosynthesis, respiration, calcification, and $CaCO_3$ dissolution (Albright et al., 2015; Cyronak et al., 2018; Gattuso et al., 1993, 1996; Kinsey, 1978, 1985). Photosynthesis increases pH and DO concentrations, while respiration decreases these parameters. Calcification and $CaCO_3$ dissolution decrease and increase pH, respectively, with no direct influence on DO. These processes occur within both benthic and water column communities (Kinsey, 1985; Pezner et al., 2021; Smith et al., 2013; Tilstra et al., 2018). The degree to which the biogeochemistry of reef seawater is modified depends on the relative rates of these processes, which vary over diel (Gruber et al., 2017; Kekuewa et al., 2021) and seasonal timescales (Davis et al., 2020; Page et al., 2019), and the benthic communities modifying the overlying seawater (e.g., seagrass, seaweed, sand, rubble, and corals; Jokiel et al., 2014; Page et al., 2016). Rates of photosynthesis and calcification generally increase with incident light (Cohen et al., 2016; Sawall & Hochberg, 2018), although light-induced changes in photosynthetic rate may also be influenced by the photoadaptive ability of the coral (Anthony & Hoegh-Guldberg, 2003). Additionally, the range of variability in reef seawater biogeochemistry appears to partly scale with depth (Cyronak et al., 2020; Page et al., 2019), but with strong influence from the local hydrodynamics (Falter et al., 2013; Kekuewa et al., 2021; Mongin & Baird, 2014; Zhang et al., 2011, 2012). The magnitude of biogeochemical variability is also affected by seawater flow rate and trajectory (i.e., the path the water takes across the reef), which determine the habitats seawater intersects, the time the seawater is in contact with the benthos, and the amount of mixing and dilution that occurs between open

ocean and other water masses (Falter et al., 2013; Gruber et al., 2017; Lowe & Falter, 2015; Winter et al., 2020). Seawater flow also affects the rates of metabolic processes by alleviating mass-transfer limitation (Dennison & Barnes, 1988; Falter et al., 2004), which may influence the response of corals to ocean warming (Edmunds & Burgess, 2017; Rogers et al., 2016) and acidification (Comeau et al., 2014). Reef seawater circulation and biological drivers of biogeochemical variability are therefore inextricably linked within coral reef systems and must be characterized for coral reef biogeochemical variability to be fully understood.

Breaking waves have been recognized as the primary forcing of seawater circulation on many coral reefs since the mid 20th century (Lowe et al., 2009b; Munk & Sargent, 1948; Symonds et al., 1995), though tides (Dumas et al., 2012), winds (Kraines et al., 1999; Lowe et al., 2009a), and buoyancy differences (Monismith, 2007) can also play important roles. As waves shoal and break on the reef crest, the mean water level increases within the surf zone (i.e., wave setup), creating a pressure gradient that drives seawater flow over the reef flat and into the lagoon (Lowe et al., 2009a; Munk & Sargent, 1948; Taebi et al., 2011; Vetter et al., 2010). This increase in mean water level within the surf zone is balanced on the offshore side by the radiation stress gradient created by the transfer of momentum from breaking and shoaling waves into the water column (Longuet-Higgins & Stewart, 1962), and on the onshore side by the friction of the reef flat. The magnitude of the wave setup and the resulting speed and direction of flows generated for a given wave condition are determined by the geomorphology and friction of the reef system (Falter et al., 2013; Lentz et al., 2016; Lindhart et al., 2021; Monismith et al., 2013; Vetter et al., 2010).

In this study, the main goal was to assess how daily variations in incident light and reef seawater circulation affected the magnitude of diel variability in seawater pH and DO at contrasting reef habitats (reef flat, lagoon, and outflow channel) on a fringing coral reef system in Okinawa, Japan over a 3-week period. The results highlight the important role physical drivers play in modulating biogeochemical variability on fringing reef systems and serve as a starting point for developing predictive capacity at the local scale.

2. Materials and Methods

2.1. Field Site Description

This study was conducted on a fringing coral reef near Onna-son, Okinawa, Japan (26.449720°N, 127.794245°E, Figure 1a) in October 2019. This timing allowed us to observe the Onna-son system under high flow and moderate light conditions while reducing the likelihood that the study would be impacted by typhoons. The reef system consists of a forereef characterized by spur and groove formations that rises to a reef flat approximately 2.8 km long and 150 m wide, with a mean depth of approximately 1.3 m. The reef flat is composed of a flat, tightly consolidated pavement covered by crustose coralline algae, sand, small chunks of rubble, and turf algae. Small coral colonies are present within holes in the framework. Behind the reef lies a lagoon (depth = 3–4 m) ranging from 600 to 1,500 m wide. The lagoon benthos consists predominantly of sand, seagrass, and coral rubble, with several small patch reefs as well as several coral and seaweed farms (Figure S1 in Supporting Information S1). The lagoon is primarily connected to the open ocean through a ∼100 m wide, 12–15 m deep channel in the north and a complex system of deeper channels (depth >20 m) and patch reefs in the south. A smaller, ∼5 m deep channel runs through the center of the lagoon to service the Maeganeku fishing port. Channel depths were estimated using Google Earth Engine after (Li et al., 2021), based on Sentinel-2 surface reflectance.

2.2. Measurement of Waves, Currents, and Wave Setup

An array of current meters and pressure sensors were deployed between 10–29 October to measure seawater flow speed, direction, and wave setup (see Table 1 and Figure 1b for deployment settings and locations). In addition, significant wave height and period were estimated hourly on the forereef based on pressure measurements from two 2 MHz Nortek Aquadopp acoustic Doppler current profilers (ADCPs, C7 and C8) while waves on the reef crest and back reef were measured continuously by two RBR Virtuoso pressure sensors (2 Hz; P1 and P2). Waves on the reef flat were measured hourly by a Nortek Vector acoustic Doppler velocimeter (ADV, C1). Current profiles were measured using two 2 Mhz Aquadopps (C7 and C8), three 1 Mhz Aquadopps (C2, C3, and C6), and two Teledyne RDI Sentinel Versus (C4 and 5) with bin sizes ranging from 0.3 to 1 m. All current meters burst sampled at 1 Hz but had different burst durations and intervals due to the different memory and battery life

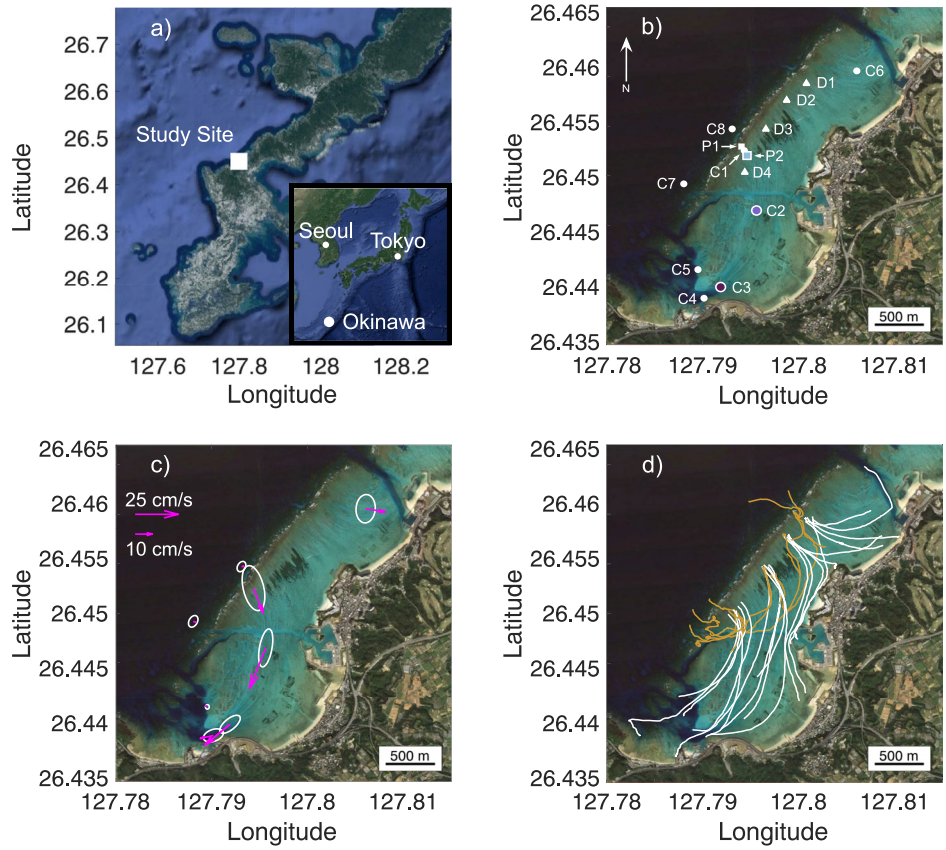

Figure 1. (a) Location of study site and Okinawa (inset). (b) Instrument deployment locations in Onna-son, Okinawa, Japan. Points labeled C represent current meters (circles), points labeled P represent pressure sensors (squares), and points labeled D denote drifter deployment locations (triangles). Colored symbols denote points at which pH, dissolved oxygen, salinity, and temperature measurements were obtained in addition to physical sensors. Photosynthetically active radiation was measured at C1. See Table 1 for full instrument deployment details. (c) Time and depth averaged Eulerian current vectors (pink) and principal component ellipses (white, radii represent one current velocity standard deviation). (d) Drifter tracks under high flow (C2 speed >15 cm/s, white) and low flow (C2 speed <15 cm/s, orange). Under high flow conditions, drifters tracked benthic striations visible in Google Earth Pro imagery.

capacities of each instrument (Table 1). Forereef sensors were deployed later than lagoon and channel sensors due to wave related safety concerns and logistical constraints.

2.3. Drifter Deployments

Drifter deployments were conducted using Pacific Gyre reef drifters on 16, 17, 21, and 22 October with multiple deployments being conducted on all days except 22 October. During each deployment, one drifter was released at each of the points D1–D4 (Figure 1b) in quick succession and allowed to drift until they became caught on the shoreline, left the reef system, or time constraints forced us to recover the drifters. The position of each drifter was recorded every minute via the drifters' iridium telemetry.

2.4. Biogeochemical Measurements

Seawater temperature (T), salinity (S), pH, and DO were measured every 30 min at stations P2, C2, and C3, forming a transect from the back reef to the southern channel that roughly followed the predominant flow trajectory (Figure 1b). These parameters were measured by a SeapHOx (Bresnahan et al., 2014) at P2, and by pairing a SeaFET (pH) and a Seabird SBE 16 plus V2 SeaCAT recorder (T, S) equipped with an oxygen optode (Aanderaa Oxygen Sensor 3835) at C2 and C3. pH sensors were cross calibrated prior to deployment, however the oxygen

Table 1
Instrument Locations, Configurations, and Deployment Information From the Study Period in October 2019

Site	Instrument	Approximate depth (m)	Blanking distance (m): bin size (m)	Parameters measured	Sampling scheme	Deployment dates
C1	ADV	0.8	0.157:NA	Currents	300 samples every hour	10–29 October
	PAR sensor	0.8	–	Photosynthetically Active Radiation	10 samples every 30 min	
C2	Aquadopp (2 MHz)	2.8	0.2:0.3	Currents	10 samples every 5 min	10–29 October
	SeaFET	2.8	–	pH	1 sample every 30 min	
	Seabird	2.8	–	T, S, DO	1 sample every 30 min	
C3	Aquadopp (1 MHz)	6.6	0.4:1.0	Currents	10 samples every 5 min	10–29 October
	SeaFET	6.6	–	pH	1 sample every 30 min	
	Seabird	6.6	–	T, S, DO	1 sample every 30 min	
C4	Sentinel (1 MHz)	9.3	0.4:1.0	Currents	120 samples every 15 min	21–29 October
C5	Sentinel (1 MHz)	13.5	0.4:1.0	Currents	120 samples every 15 min	17–29 October
C6	Aquadopp (2 MHz)	2.8	0.2:0.3	Currents	10 samples every 5 min	10–29 October
C7	Aquadopp (1 MHz)	8.0	0.2:0.3	Currents	60 samples every 15 min	17–29 October
				Waves	1,024 samples every hour	
C8	Aquadopp (1 MHz)	8.5	0.2:0.3	Currents	60 samples every 15 min	17–29 October
				Waves	1,024 samples every hour	
P1	RBR Virtuoso	1.3	–	Pressure	Continuous at 2 Hz	10–29 October
	SeapHOx	1.3	–	pH, T, S, DO	1 sample every 30 min	
P2	RBR Virtuoso	1.8	–	Pressure	Continuous at 2 Hz	10–29 October

Note. The differing deployment dates were a result of logistical and physical constraints preventing all instruments from being deployed at once. Sampling schemes were developed based on the parameters being measured, and the memory and battery constraints of the different instruments. All current meters burst sampled at 1 Hz according to the stated sampling scheme.

optodes were not. An ECO-photosynthetically active radiation (PAR) sensor (Wetlabs, Seabird Scientific) measured PAR at C1. The pH measurements were calibrated on the total pH scale based on discrete bottle samples taken next to the sensors during deployments and were estimated to have accuracies of ±0.025 units (P2), ±0.003 units (C2), and ±0.011 units (C3). The SeapHOx and Seabird salinity and temperature sensors were factory calibrated. The reported salinity and temperature accuracy for the SeapHOx was ±0.00084 at 25°C, and ±0.002°C, while the reported accuracy for the Seabird for the same parameters were ±0.0015°C and ± 0.005°C. The Aanderaa Oxygen Sensor 3835 has a reported accuracy of ±5% or ±8 μM and a precision of ±4 μM. DO and pH data were salinity corrected using salinity values from the SeapHOx (P2) and Seabirds (C2 and C3).

3. Data Processing and Analyses

3.1. Pressure, Currents, and Wave Setup

Pressure data from P1, P2, and C8 were analyzed by dividing each burst into 18 segments of equal length with 50% overlap, applying a Hann window (Hann, 1903) to the segments and computing spectra. The resulting spectra had a frequency resolution of 0.01 Hz and were used to obtain the peak period, T_P, for each burst. Significant wave heights H were calculated as $H = 4\sqrt{m_0}$ where m_0 is the zeroth moment of the spectra in the wind wave frequency band (0.04 Hz $< f <$ 0.3 Hz), while root mean squared wave heights were computed as $H_{RMS} = 0.706H$.

Current measurements were obtained by averaging all samples in a burst and averaging over the full depth to produce a Eulerian velocity time series, u. Currents measured at C1 were not depth averaged, as ADVs measure velocity at a single point. u time series were rotated into the direction of the mean flow, with positive flow representing cross reef flow (C1), flow from the reef flat toward the channels (C2, C3, C4, and C6), or north-easterly alongshore flow (C7 and C8). Subtidal velocity time series were calculated by applying a Godin filter to u

to remove the influence of diurnal and semi-diurnal tidal components, and any other components with higher frequencies (Godin, 1972).

Wave setup was calculated from 15-min averages of water level at C8, P1, and P2 following Vetter et al. (2010). We took the setup at C8 to be 0 cm (though see below), and so the difference in mean depth between C8 and P1 and P2 respectively at each timestep is given by

$$\mathrm{d}\overline{h_{\mathrm{Pi}}} = \overline{h_{\mathrm{Pi}}} - \overline{h_{\mathrm{C8}}}, \quad (i = 1, 2) \tag{1}$$

We subsequently performed a regression of the form

$$\mathrm{d}\overline{h_{\mathrm{Pi}}} = aH_{S_{\mathrm{C8}}} + bt + c \tag{2}$$

where $H_{S_{\mathrm{C8}}}$ is the observed significant wave height at C8 and t is time. This regression relates the measured difference in depths between C8 and P1 or P2 with the incident significant wave height, while accounting for drifts in the pressure sensor over time (b) and giving an offset (c) such that setup is zero when significant wave height is zero (See Table S1 in Supporting Information S1 for regression results). The resulting setup at each site can then be estimated using the coefficients derived in Equation 2 as

$$\eta_{\mathrm{Pi}} = \mathrm{d}\overline{h_{\mathrm{Pi}}} - bt - c, \quad (i = 1, 2) \tag{3}$$

We estimated the setdown $\tilde{\eta}$ at C8 for each time point as (Longuet-Higgins & Stewart, 1962)

$$\tilde{\eta} = -\frac{H_{S_{\mathrm{C8}}}^2 k}{8 \sinh 2 k \overline{h_{\mathrm{C8}}}} \tag{4}$$

where $H_{S_{\mathrm{C8}}}$ is the significant wave height at C8, k is the wave number and $\overline{h_{\mathrm{C8}}}$ is the 15-min average depth at C8. The estimated setdown was found to be small and estimates of setup at P1 and P2 referenced to $\overline{h_{\mathrm{C8}}} - \tilde{\eta}$ did not differ significantly from estimates referenced to $\overline{h_{\mathrm{C8}}}$ as above. The absence of another offshore pressure sensor in line with C8, P1, and P2 prevented us from making direct measurements of the setdown.

3.2. Diel Variability in pH and Dissolved Oxygen

Daily daytime variability in pH ($\Delta\mathrm{pH}_{\mathrm{day}}$) and DO ($\Delta\mathrm{DO}_{\mathrm{day}}$) for each site was calculated as the difference between the daily maximum and the mean of each parameter for the entire time series. The means of the time series were used instead of pre-dawn values to minimize the impact of the previous night's variability on the daytime variability calculated for the following day. Similarly, nighttime variability ($\Delta\mathrm{pH}_{\mathrm{night}}$ and $\Delta\mathrm{DO}_{\mathrm{night}}$) was calculated from the difference between the daily minimum and the mean for the time series. Calculating variability as the difference between the pre-dawn and maximum daily values, or dusk and nightly minimum values could lead to large variabilities being estimated for days that reached typical maximum pH or DO values but were preceded by a night that reached abnormally low pH or DO values. This would be appropriate for systems with long residence times in which these changes could be attributed to reef metabolism, however, the Onna-son reef had a residence time on the order of hours during the study period such that much of the nighttime (or daytime) signal is likely to be advected out of the reef system and have little impact on the maximum (or minimum) pH or DO value reached during the following day (or night). $\Delta\mathrm{pH}_{\mathrm{day}}$ and $\Delta\mathrm{DO}_{\mathrm{day}}$ were assessed as a function of the mean PAR and inverse mean current speed ($\overline{u^{-1}}$) from the corresponding day using multiple linear regression (MLR). Inverse mean speed was used as a variable because the degree to which the biogeochemistry of a seawater parcel is modified is proportional to the amount of time it spends on the reef, or its residence time (Smith & Key, 1975; Venti et al., 2012). MLR models were fit with and without interaction terms and the model with the highest adjusted R^2 value was selected. Similar analyses were performed on the decreases in pH and DO at each site at night, though simple linear regressions of $\Delta\mathrm{pH}_{\mathrm{night}}$ and $\Delta\mathrm{DO}_{\mathrm{night}}$ as a function of $\overline{u^{-1}}$ were performed as there was no PAR. Assumptions of linearity, multicollinearity, and residual normality were assessed and met by each model.

4. Results

4.1. Waves, Wave Setup, and Lagoon Currents

Tides were mixed-semidiurnal, with a mean range of 1.37 ± 0.42 m (mean ± 1 SD) and a maximum range of 2.10 m (Figure 2). The reef flat was occasionally exposed during low tide. Significant wave height H_S measured at the forereef varied from 0.2 to 1.6 m with a mean of 0.8 ± 0.3 m (mean ± 1 SD) and peak period T_P ranged from 3.5 to 9 s with a mean of 7.61 ± 0.75 s (mean ± 1 SD). The largest H_S was observed on 24 October, and the longest T_p was measured on 24, 25, and 27 October. Waves were consistently from the northwest (321° ± 7°, mean ± 1 SD) and were onshore as the reef flat faced the northwest (~305°).

Wave setup ranged from 0.7 to 9.0 cm and 0.8–7.6 cm at P1 and P2 respectively (Figure 2) and demonstrated a clear tidal signal, with setup being greatest during low tide at both sites. Setup at P1 was greater than at P2 during low tide, creating an onshore pressure gradient across the reef flat. At high tide, setup was similar at both sites and produced small pressure gradients that acted in either direction at different points in the time series. Setup increased with offshore significant wave height (Figures 3a and 3b). Wave setup was assessed as a function of incident wave energy and seawater depth using MLRs and found to be strongly correlated with these predictive variables at both sites, with adjusted R^2 values of 0.92 and 0.85 for setup at P1 and P2 respectively (Figures 3a and 3b, Table S3 in Supporting Information S1). A significant interaction was found between the effects of water level and incident wave energy on the resulting wave setup at both P1 and P2, with the difference between the setups observed at high tide and low tide increasing at higher incident wave energy fluxes (greater setups at low tide, smaller setups at high tide).

On average, circulation within the reef system was dominated by two distinct circulation cells in the north and south of the lagoon respectively. In both cells, the predominant flow tracked benthic striations visible in Google Earth imagery (Figure 1c). Both cells comprised seawater flowing into the lagoon over the reef crest and exiting through channels. The tracks of drifters released from D1 and D2 (Figure 1b) suggested that the boundary between these two cells moved, but typically lay between these points. We could not determine what controlled the location of this boundary.

Except for 23–27 October, the circulation in the southern cell (C1–C5) was highly consistent for the duration of the study, with mean flows roughly aligned with the principal component axes (Figure 1c). The direction of the flow in the northern cell (C6) was more variable, with onshore flow during flood tides (121° ± 47°, mean ± 1 SD) and channel-ward flow during ebb tides (97° ± 47°, mean ± 1 SD, Figure 4, see also drifter tracks in Figure 1c).

Measured flow speeds were higher at C1 ($u_{C1} = 17 \pm 14$ cm/s), C2 ($u_{C2} = 26 \pm 13$ cm/s), and C3 ($u_{C3} = 20 \pm 10$ cm/s) than at C6 ($u_{C6} = 14 \pm 8$ cm/s). Flow speeds measured at C5 were much lower than at the other sites within the lagoon ($u_{C5} = 2 \pm 2$ cm/s).

Flow speeds in the mean flow direction were significantly correlated ($p < 0.001$ at all sites) with incident wave energy flux alone (C3, $R^2 = 0.71$; C4, $R^2 = 0.88$, Figures 3e and 3f), or both incident wave energy flux and tide (C1, $R^2_{Adj} = 0.72$; C2, $R^2_{Adj} = 0.72$; C5, $R^2_{Adj} = 0.20$; C6, $R^2_{Adj} = 0.63$. See Figure 3c, 3d, 3g and 3h, and Table S3 in Supporting Information S1 for full regression results). Significant interactions ($p < 0.05$) between incident wave energy flux and water level were found at C1, C2, and C6. Flow speeds at C3 and C4 were correlated with the square root of the incident wave energy flux, while linear relationships were observed at all other sites (Table S3 in Supporting Information S1). Current speeds perpendicular to the direction of the mean flow were weakly correlated with incident wave energy at all sites ($R^2 < 0.05$ at all sites). Flow speed varied at near tidal frequencies at C1, C2, C3, and C6, but the magnitude of this variation and the relationship between tide and speed differed between the sites (Figure S2 in Supporting Information S1). The fastest speeds observed at C1 and C6 occurred during low tide, while the fastest speeds at C3 occurred during ebb tides. The oscillations in flow speed at C2 appeared to be out of phase with the tide, with higher flow speeds occurring at low tide before 14 October and after 25 October, but greater flow speeds being measured during high tides in the intervening period (Figure S2 in Supporting Information S1).

Flow direction became more consistent with increasing speed at all sites within the lagoon (Figure 4), though the direction and strength of this relationship varied between sites. The consistency in the direction of high-speed flows was greatest at C1, C2, C3, and C4, while there was a weaker effect at C5. Flow direction reversed at C3 and C4 on 17, 21, 22, 23, 26, and 28 October. Flow direction at C6 in the northern lagoon also became more

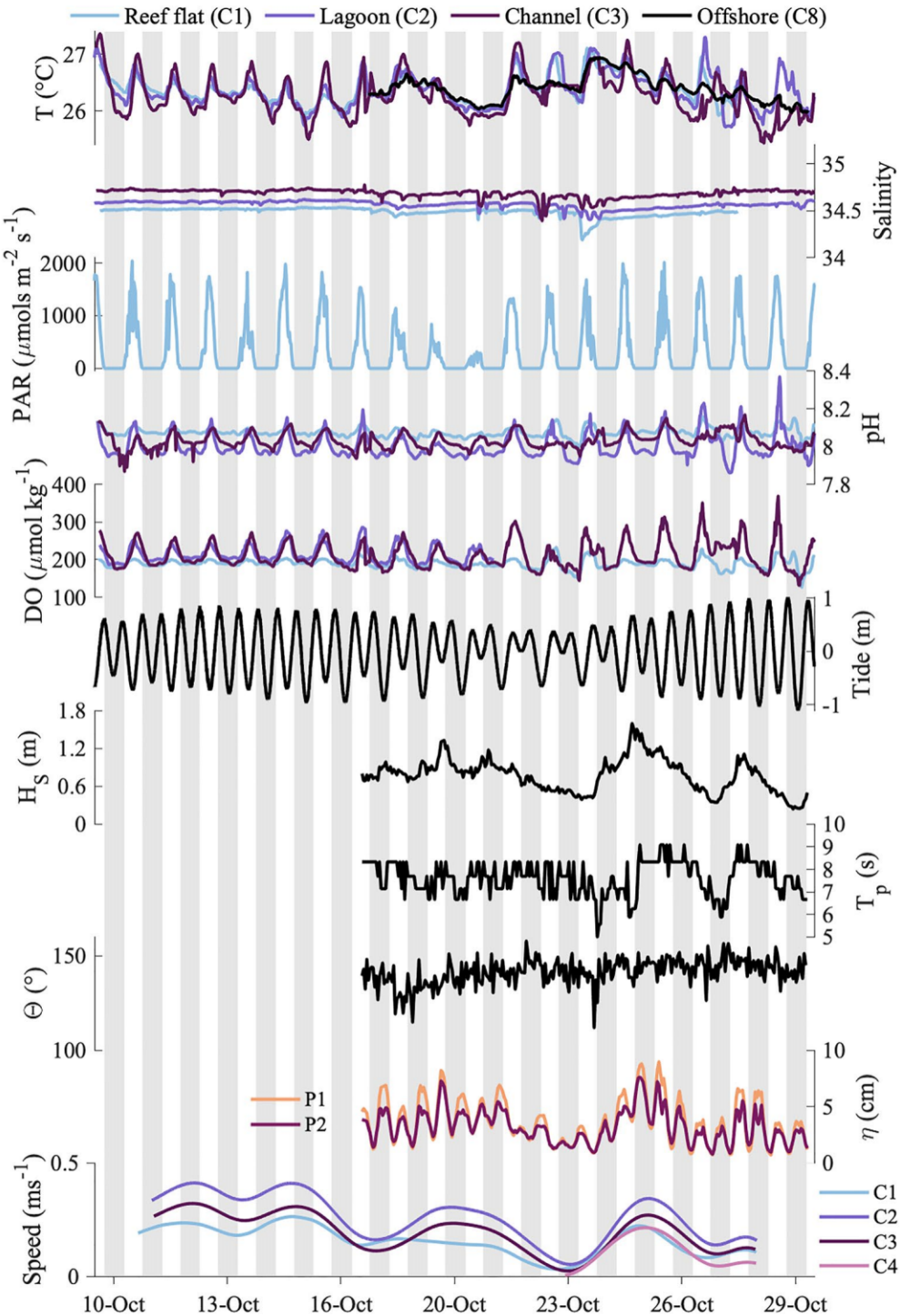

Figure 2. Temporal variability in seawater temperature (T), salinity, photosynthetically active radiation, pH, dissolved oxygen (DO), relative tide, offshore significant wave height (H_S), peak wave period (T_p), incident wave direction (θ), reef flat wave setup (η), and subtidal speeds within the lagoon from 10–29 October. Gray bands represent nighttime. Logistical and physical constraints prevented forereef sensors from being deployed early in the study period, resulting in shorter time series for H_S, T_P, and θ. The DO sensor in the lagoon became biofouled and so only data until 20 October are reported (see Table 1 for full deployment details).

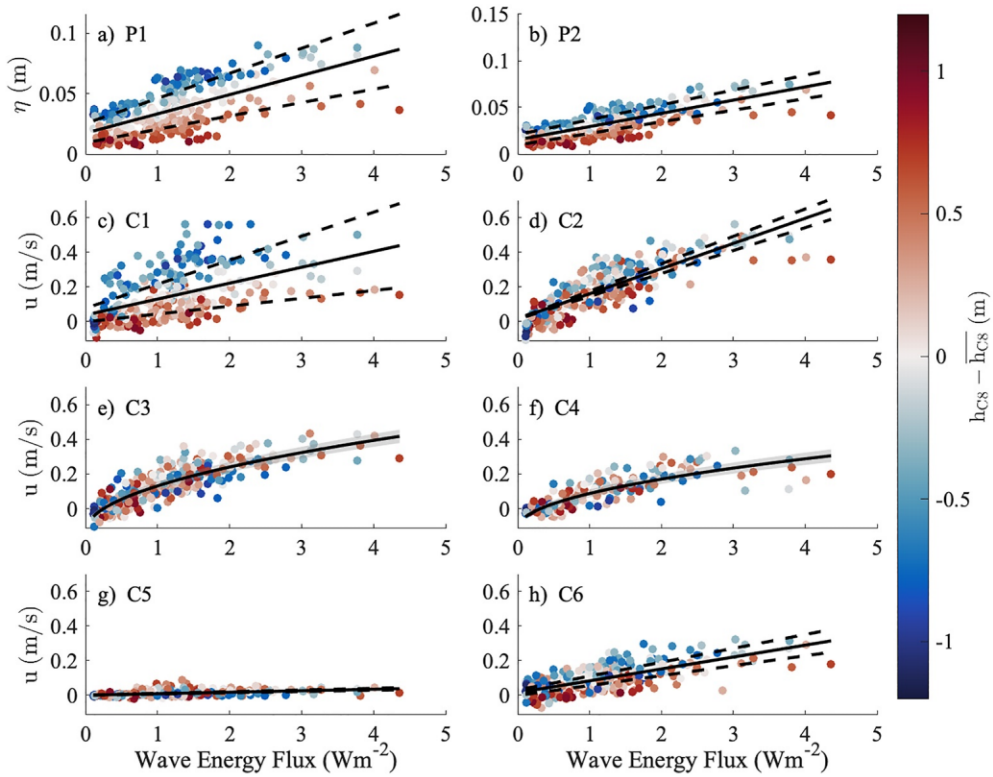

Figure 3. Setup (η) at P1 (a) and P2 (b), and flow speed at C1–C6 (c–h) as a function of the incident wave energy flux. Colors represent the water level at C8 for each wave measurement period standardized to the mean depth at C8 for the entire study period such that red colors represent high tides and blue colors represent low tides (relative to the mean). In panels (a–d), (g), and (h), solid lines represent significant regressions at the mean water level at C8 for the time series, while the dashed lines show the relationship at the mean water level at C8 ± the standard deviation of the water level. Solid lines and shading in panels e and f represent significant regressions and 95% confidence intervals. See Table S3 in Supporting Information S1 for full regression results.

consistent at higher flow speeds, but to a lesser degree than the southern sites. The direction of flow was increasingly onshore (dashed black lines, Figure 4) during rising tides and more offshore during falling tides at each site. The increased consistency of flow direction at high speeds was also observed in the drifter data, with drifters released on high flow days (defined as daily mean flow at C2 > 15 cm/s) moving from the reef crest to the channels and drifters released during slow flow days traveling more variable paths (Figure 1d).

Offshore currents were weaker than those within the lagoon ($u_{C7} = 6 \pm 3$ cm/s, $u_{C8} = 6 \pm 3$ cm/s), though this could be a result of the lagoon current meters measuring the complete water column while the offshore current meters did not sample the upper few meters of the water column. Flows at both C7 and C8 were predominantly alongshore and moved toward the southwest during rising tides and the northeast during falling tides.

4.2. Temperature, Salinity, PAR, pH, and Dissolved Oxygen

Mean daily PAR was highest at the start and end of the time series and lowest on 20 October (Figure 2). The PAR sensor was deployed on the shallow reef flat and therefore measured higher levels of irradiance than experienced at the benthos at the other, deeper reef sites. We did not observe marked differences in turbidity between the sites, and Grossmann et al. (2015) observed low turbidities on a nearby coral reef except during typhoon conditions. Given the relatively small size of the study area, we assumed that the general trends observed in these data were representative of reef-wide conditions, although the absolute value of the benthic PAR intensity at each site would differ due to attenuation at depth. Day length decreased from 11:40 to 11:15 hr over the course of the study.

The seawater temperature at the reef flat, lagoon, and channel (sites C1–C3) varied between 25.43°C and 27.36°C during the study period and mostly exhibited a clear diel cycle (Figure 2). The channel was on average slightly

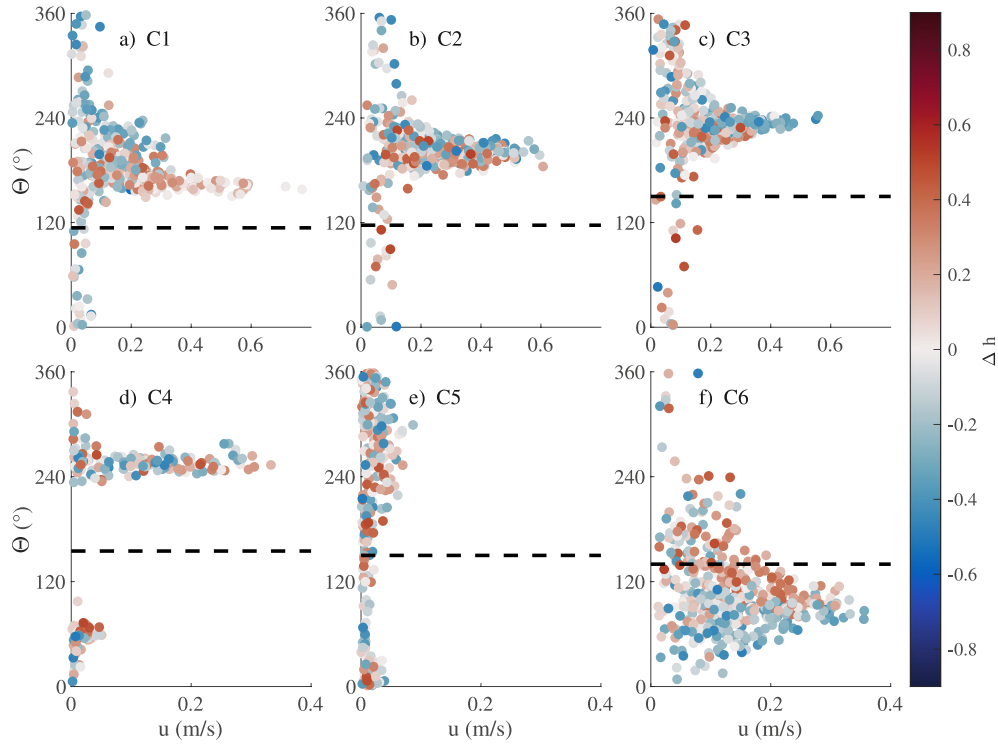

Figure 4. Flow direction (θ) as a function of flow speed (U) at C1–C6 (a–f). The color of each point represents the change in depth relative to the previous measurement with red indicating rising tides and blue indicating falling tides. Dashed lines represent the direction of onshore flow, which varied slightly between each site. At sites C1–C3, C5, and C6, flow during rising tides (red points) was more aligned with the onshore direction than flows during falling tides (blue points).

cooler but more variable (T_{C3} = 26.27°C ± 0.36°C, mean ± 1 SD) than the reef flat (T_{P1} = 26.40°C ± 0.24°C) or lagoon (T_{C2} = 26.37°C ± 0.30°C). However, during the day the channel was the warmest site and the reef flat the coolest while the opposite was observed at night. The magnitude of diel seawater temperature variability was highest on 10, 15, 21, and 26 October, and smallest on 20 October. On several nights (i.e., 10 and 11 October), small nocturnal increases in seawater temperature were observed during rising tides.

Salinity was largely invariable at each site (S_{C1} = 34.49 ± 0.05, S_{C2} = 34.57 ± 0.04, S_{C3} = 34.69 ± 0.05, mean ± 1 SD), except for large (~0.2) decreases observed after rainfall events (Figure 2). Decreases were initially observed on the reef flat, then subsequently in the lagoon and channel, with the magnitude of the decrease generally increasing with distance from the reef crest. Conversely, the greatest decrease was observed on the reef flat on 23 October following 9.6 mm of rain falling over 2 days. Following precipitation events, salinity initially increased rapidly at each site before rising more gradually over the course of several days to pre-precipitation event values.

Seawater pH and DO exhibited clear diel signals at all sites (Figure 2). For both parameters, variability was greater within the lagoon (pH_{C2} = 8.00 ± 0.06, DO_{C2} = 211 ± 35 µmol kg^{-1}, mean ± 1 SD) than the channel (pH_{C3} = 8.03 ± 0.04, DO_{C3} = 214 ± 22 µmol kg^{-1}) or the reef flat (pH_{P1} = 8.08 ± 0.02, DO_{P1} = 189 ± 13 µmol kg^{-1}). Mean pH was highest on the reef flat and lowest within the lagoon. The oxygen sensors were not cross-calibrated under identical conditions, potentially introducing differences in absolute values and limiting comparisons to the relative variability between sites. Diel pH and DO variability (whether characterized as the difference of the extremes relative to the time series mean, daily maximum or nightly minimum values, or the difference between the daily maximums and minimums) was relatively consistent at all sites from 10–17 October, before decreasing to a minimum on 20 October. The diel variability in both parameters subsequently increased after 20 October and exhibited greater interdaily variability than was observed between 10–17 October. While pH generally decreased at night, temporary increases in nighttime pH were observed at the reef flat and lagoon sites (C1 and C2) but were not prominent in the channel or coincident with increases in the DO data. Unfortunately, the DO sensor in the lagoon (C2) became biofouled later in the deployment, and only data before 21 October are presented.

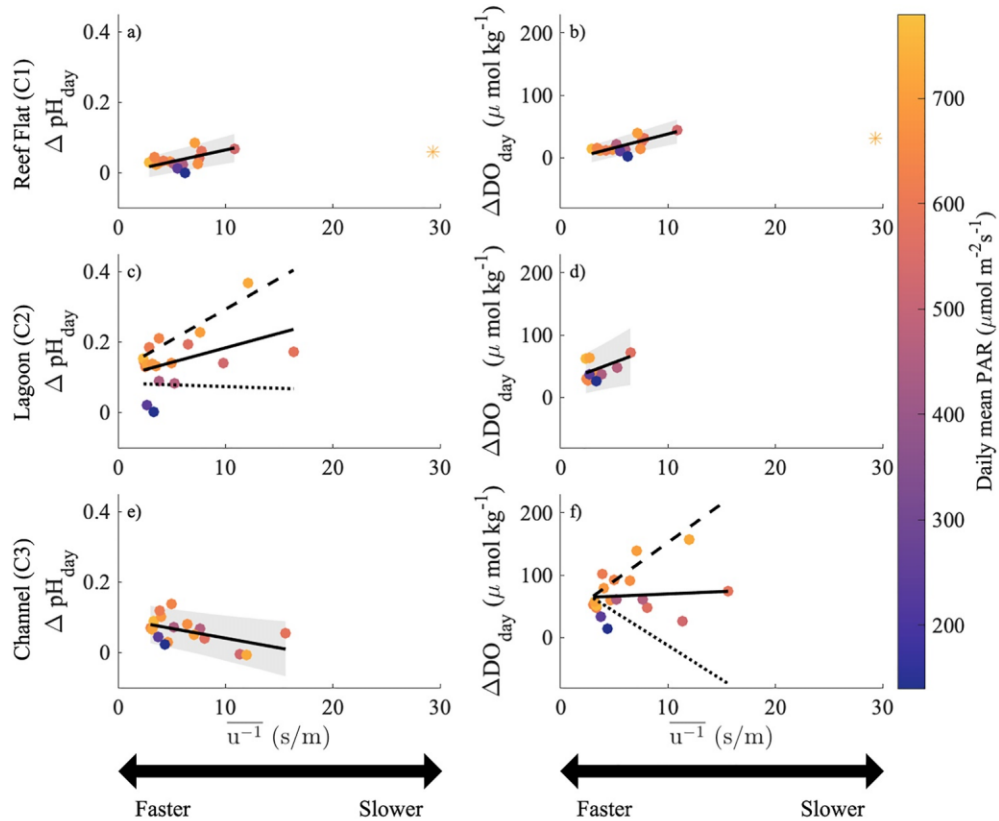

Figure 5. Daytime increases in pH and dissolved oxygen as a function of inverse mean flow speed within the reef flat (C1, a, b), lagoon (C2, c, d), and channel (C3, e, f) sites throughout the study period. Colors represent mean photosynthetically active radiation (PAR) for the corresponding day. In panels (a), (b), (d), and (e) solid lines and shading represent significant regressions and 95% confidence intervals for ΔpH or ΔDO against inverse flow speed at the mean daily mean PAR value (581 μmol m^{-2} s^{-1}) as there was no significant interaction between inverse flow speed and incident PAR. In panels c and f, solid lines show the regression at the mean daily mean PAR value, while the dashed and dotted lines represent regressions at the mean daily PAR ± the standard deviation of mean daily PAR (166 μmol m^{-2} s^{-1}), respectively. Regressions run without high leverage points (stars, far right of a, b) are presented for the reef crest (see Table 2 for full regression results).

4.3. Diel Variation in pH and Dissolved Oxygen in Relation to PAR and Current Speed

4.3.1. Day

Like the overall variability in pH and DO, the largest daytime increases in these parameters occurred in the lagoon and in the channel, respectively, with the smallest increases in both parameters occurring at the reef flat (Figure 5). For the reef flat, MLRs of ΔpH_{day} or ΔDO_{day} performed as a function of inverse mean flow speed ($\overline{u^{-1}}$) and mean PAR were statistically significant ($p < 0.05$) and accounted for 44% and 52% of the observed variability, respectively (Table 2). However, the regressions appeared strongly influenced by isolated, high leverage points from 28 October (stars, Figures 5a and 5b; Cook's Distance > 1). Exclusion of these points improved model predictability for both ΔpH_{day} (59%) and ΔDO_{day} (69%) (Figures 5a and 5b; Table 2). The MLR of the lagoon data was significant with respect to ΔpH_{day} ($p < 0.01$), with $\overline{u^{-1}}$ and mean PAR explaining 74% of the variability when an interaction term was included (Figure 5c, Table 2). In contrast, no significance was found with respect to ΔDO_{day}, though it should be noted that this time series was abbreviated by the sensor becoming biofouled toward the end of the deployment (Figure 5d). In the channel, MLR models were statistically significant with respect to both ΔpH_{day} and ΔDO_{day} ($p < 0.05$), with $\overline{u^{-1}}$ and mean PAR explaining 25% of ΔpH_{day} variability and 68% of ΔDO_{day} variability (Figures 5e and 5f, Table 2). Notably, channel ΔpH_{day} was negatively correlated with $\overline{u^{-1}}$. The channel ΔDO_{day} data were best fit by a model with an interaction term. The interaction terms present in the lagoon ΔpH_{day} and channel ΔDO_{day} indicate that the effect of daily mean PAR on these parameters changes with flow speed. For example, an increase in daily mean PAR of 100 μmol m^{-2} s^{-1} would increase lagoon ΔpH_{day} by

Table 2
Results for Multiple (Day) and Simple (Night) Linear Regressions of the Maximum Deviations in pH and Dissolved Oxygen (DO) From the Timeseries Mean for Each Day and Night Against Inverse Mean Speed and Photosynthetically Active Radiation (PAR, During the Day Only)

	Site	Parameter	R^2 (see caption)	Model p value	Model f statistic	Intercept (±s.e.)	Inverse daily mean speed coefficient (±s.e.)	PAR coefficient (±s.e.)	Interaction term coefficient (±s.e.)
Day	Reef flat	ΔpH_{day}—all points	**0.44**	**0.011**	5.37	−0.14 ± 0.064	**0.022 ± 0.010**	**−0.00024 ± 0.000090**	**−0.000029 ± 0.000014**
		ΔpH_{day}—excl. high leverage	**0.59**	**<0.001**	12.6	**−0.049 ± 0.017**	**0.0067 ± 0.0016**	**0.000081 ± 0.000021**	NA
		ΔDO_{day}—all points	**0.52**	**0.040**	7.07	**−96.8 ± 31.6**	**17.2 ± 5.0**	**0.16 ± 0.045**	**−0.023 ± 0.007**
		ΔDO_{day}—excl. high leverage	**0.69**	**<0.001**	18.5	**−24.9 ± 8.0**	**4.4 ± 0.76**	**0.032 ± 0.0097**	NA
	Lagoon	ΔpH_{day}	**0.74**	**<0.001**	15.4	0.04 (0.089)	−0.024 (0.025)	0.00010 (0.00015)	0.000056 (0.000056)
		ΔDO_{day}	0.35	0.092	3.43	−0.76 ± 17.8	6.4 ± 3.3	0.043 ± 0.022	NA
	Channel	ΔpH_{day}	**0.25**	**0.046**	3.82	0.056 ± 0.032	**−0.0055 ± 0.0022**	0.000068 ± 0.000048	NA
		ΔDO_{day}	**0.68**	**<0.001**	13.2	**180.2 ± 51.2**	**−40.0 ± 10.2**	**−0.2 ± 0.083**	**0.07 ± 0.017**
Night	Reef flat	ΔpH—all points	**0.58**	**<0.001**	20.4	−0.0088 ± 0.0047	**−0.0025 ± 0.00055**	NA	NA
		ΔpH—excl. high leverage	0.23	0.059	4.21	−0.012 ± 0.0058	−0.0018 ± 0.00088	NA	NA
		ΔDO—all points	**0.78**	**<0.001**	52.6	−0.039 ± 1.78	**−1.5 ± 0.21**	NA	NA
		ΔDO_{night}—excl. high leverage	**0.57**	**<0.001**	18.6	−0.20 ± 2.30	**−1.5 ± 0.35**	NA	NA
	Lagoon	ΔpH_{night}—all points	**0.72**	**<0.001**	38.7	−0.039 ± 0.0052	**−0.0043 ± 0.00068**	NA	NA
		ΔpH_{night}—excl. high leverage	0.15	0.161	2.21	**−0.041 ± 0.011**	−0.0039 ± 0.0026	NA	NA
		ΔDO_{night}—all points	**0.62**	**0.012**	11.2	−5.8 ± 5.57	**−4.9 ± 1.5**	NA	NA
		ΔDO_{night}—excl. high leverage	**0.69**	**0.011**	13.3	3.1 ± 7.11	**−7.9 ± 2.2**	NA	NA
	Channel	ΔpH	0.07	0.301	1.15	**−0.055 ± 0.014**	−0.0020 ± 0.0019	NA	NA
		ΔDO_{night}—all points	0.10	0.212	1.7	**−26.9 ± 7.09**	−1.3 ± 0.96	NA	NA
		ΔDO_{night}—excl. high leverage	**0.75**	**<0.001**	39.5	**−11.9 ± 3.9**	**−4.6 ± 0.73**	NA	NA

Note. Deviations in pH and DO were calculated by subtracting the mean of each parameter over the total time series from each parameter's daily maximum or nightly minimum. Multiple linear regressions were run with and without interaction terms and the results of the model with the higher adjusted R^2 values are presented here. Bold values are significant at $p < 0.05$. Coefficients for terms not included in the presented models are designated with NA. Adjusted R^2 and simple R^2 are reported for day and night values respectively. Note that the oxygen results from the lagoon come from a shorter data series due to the sensor becoming biofouled.

0.12 units at a flow speed of 0.05 m s^{-1} ($\overline{u^{-1}}$ = 20 s m^{-1}), but only 0.04 units at a faster flow speed (i.e., shorter residence time) of 0.2 m s^{-1} ($\overline{u^{-1}}$ = 5 s m^{-1}).

4.3.2. Night

ΔpH_{night} and ΔDO_{night} both increased in magnitude from the reef flat through the lagoon to the channel (Figure 6). Linear regressions of ΔpH_{night} as a function of $\overline{u^{-1}}$ that included all points were statistically significant ($p < 0.05$) on the reef flat and lagoon and explained 58% and 72% of the ΔpH_{night} variability at these sites, respectively (Figures 6a and 6c, Table 2). Similarly, linear regressions of ΔDO_{night} versus $\overline{u^{-1}}$ that included all points were significant ($p < 0.05$) in the reef flat and lagoon, explaining 78% and 62% of the ΔDO_{night} variability, respectively (Table 2). Performing these regressions without high leverage points (diamonds, Figures 6a–6d) resulted in non-significant relationships between $\overline{u^{-1}}$ and ΔpH_{night} at both sites, but the relationships between $\overline{u^{-1}}$ and ΔDO_{night} remained significant and explained 57% and 69% of the variability on the reef flat and lagoon, respectively

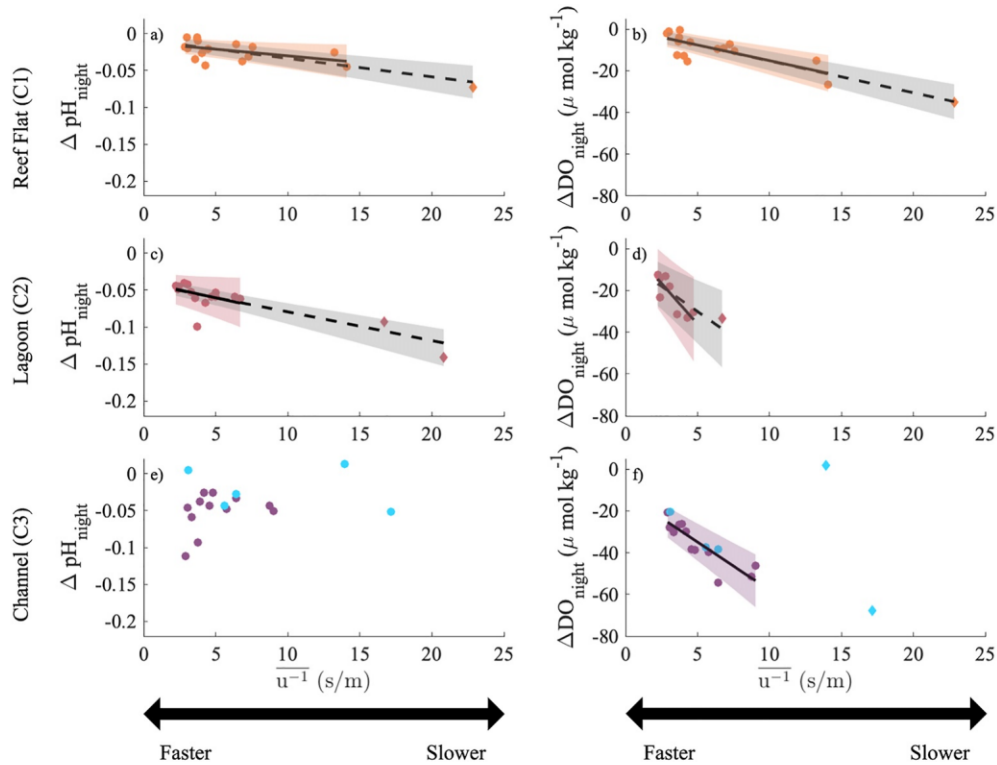

Figure 6. Nocturnal decreases in pH and DO by night-time mean inverse speed at the reef flat (C1, a, b), lagoon (C2, c, d), and channel (C3, e, f) sites. Dashed lines and gray shading in panels a-d indicate regressions and 95% confidence intervals for analyses with all datapoints, while solid lines and colored shading indicate regression lines and 95% confidence intervals of analyses conducted without high leverage points (diamonds) in all panels. Blue points in (e) and (f) indicate days during which flows reversed direction within the channel. See Table 2 for full linear regression results.

(Table 2). Regressions run with all channel points were not significant for either ΔpH_{night} or ΔDO_{night}, but regressions without high leverage points (diamonds, Figure 6f) resulted in a significant relationship between ΔDO_{night} and $\overline{u^{-1}}$ that explained 75% of the variability (Table 2).

Observations on days with high $\overline{u^{-1}}$ (i.e., low flow speeds) were limited, hence points from these days (diamonds, Figure 6) exerted a strong influence on the linear regression analyses. Exclusion of these points resulted in non-significant correlations between ΔpH_{night} and $\overline{u^{-1}}$ on the reef flat and lagoon but gave rise to a significant correlation between ΔDO_{night} and $\overline{u^{-1}}$ in the channel (Figure 6, Table 2). Linear regressions between ΔDO_{night} and $\overline{u^{-1}}$ without these high leverage points accounted for 57% and 69% of observed ΔDO_{night} variability at the reef flat and lagoon, respectively (Table 2).

5. Discussion

Here, we investigated the influence of light intensity and mean flow speed on diel pH and DO variability on a fringing coral reef in Okinawa to better understand the role physical drivers play in shaping the biogeochemical variability of coral reefs. The tidal range observed during this study (1.37 ± 0.42 m, mean ± 1 SD) was slightly higher than the mean decadal tidal range from 2011 to 2020 of 1.22 ± 0.44 m (mean ± 1 SD, Figure S3 in Supporting Information S1). While there is no long-term wave data for the Onna-son reef, significant wave height measured at the Port of Naha, a city located ~25 km southwest of Onna-son with a similar exposure, is highest from October through January, and lowest from May through July (Figure S4 and Table S2 in Supporting Information S1). Wave conditions observed during the study period are therefore likely typical of those observed in Onna-son from October through January. There are 37 days annually with daylight durations that fall within the range observed during this study (11:15–11:40 hr). During the period when Onna-son experiences a similar

wave climate to that of our study period (October–January), daylight durations range from 10:27 to 11:55 hr and are within 8% of the durations observed during this study. A lack of long-term PAR records prevented the influence of seasonal cloud cover variability on incident light intensity from being assessed.

In summary, the conditions we observed during the study period are likely representative of conditions in Onna-son from October to January. Under these conditions, statistically significant and consistent correlations were observed between flow speed, light intensity, and pH/DO changes at the reef flat, lagoon, and channel sites during both day and night, highlighting the influence these physical drivers have on regulating biogeochemical variability in coral reef habitats. However, the strength of the relationship between physical drivers and biogeochemical variability varied between parameters and sites, raising questions about the underlying factors and complexity that caused deviations from anticipated trends. In the subsequent sections, we discuss the potential factors contributing to the observed trends and differences observed between the contrasting sites.

5.1. Drivers of Reef Circulation

Our results showed that flow speed at all sites except C5 was highly correlated with incident wave energy, indicating breaking waves were the dominant driver of circulation within the Onna reef system during the study period. Consequently, observed variations in flow speed through the study site were primarily driven by changes in incident wave energy. In addition, time series of unfiltered flow speed data for all sites except C5 displayed strong tidal modulation (Figure S2 in Supporting Information S1). However, regression analyses indicated water level was only a significant predictor of flow speed at C1, C5, and C6 (Figure 3, Table S4 in Supporting Information S1). This may suggest that the interactions of waves and water level influenced current speed nonlinearly within the southern lagoon.

The dominance of waves as the primary driver of reef circulation is somewhat unexpected as the mean tidal range to significant wave height ratio (MTR:H_S) was above 1 throughout the study period (Figure S6 in Supporting Information S1), which is typical of reefs that are tidally driven (Lowe & Falter, 2015). This could indicate that the geomorphology of the Onna-son reef system allows its circulation to be wave driven at high MTR:H_S values, or that our forereef measurements did not fully capture the incident wave energy. Regardless, if the wave climates are similar between Onna-son and the nearby Port of Naha, these results suggest that the circulation of the Onna-son reef system is primarily wave driven from October through January (Figure S6 in Supporting Information S1) but may be tidally driven during the summer months.

Differences in mean flow speed at C1, C2, and C3 were likely driven by changes in the cross-sectional area of the coral reef system at each site. As seawater moved from the broad reef flat to the narrower lagoon it must have accelerated to conserve volume.

The increased variability in flow direction at slow speeds (Figure 4) may indicate that in the absence of wave forcing other factors influenced flow direction, such as wind and/or tides. However, we do not have wind data from the reef location, and no significant correlations were found between wind speeds and directions obtained from Meterological Terminal Air Report data from nearby Kadena airport and measured seawater flow speeds or directions.

The magnitude of the wave setup observed during this study was similar to other reefs backed by lagoons or open water (Lentz et al., 2016; Lowe et al., 2009b), and smaller than the setup observed on reefs that transition directly to land (Vetter et al., 2010). The presence of lagoon setup indicates that return flow from the lagoon to the open ocean was hindered by the friction of the reef system (Lowe et al., 2009b). The relationship between wave setup and water level was consistent with theory; at lower tides (shallower depths) more wave breaking and shoaling occur and reef flat friction is enhanced, producing a greater wave setup (Monismith, 2007), and vice versa at high tide. By changing the friction of the reef flat, the water level also changes the relationship between incident wave energy and the resulting setup and so creates the significant interaction observed at P1 and P2 between incident wave energy and water level. As the setup determines the resulting pressure gradients and flow speeds, the interactive effect of incident wave energy and water level on setup also likely accounts for the significant interactions observed between these factors and flow speeds at C1, C2, and C6, the three sites closest to the reef flat. The apparent reduction in wave setup observed at high incident wave energies is also a result of these tidal effects as the largest waves we observed over the entire study period happened to occur at high tide, and so produced

smaller setups than they would have at low tides. There was no significant relationship between water depth and wave height over the course of the study.

5.2. Diel Variation in pH and Dissolved Oxygen in Relation to PAR and Current Speed

Variations in PAR throughout the study period were attributable to periods of cloudy weather, while flow speed variability was primarily driven by changes in incident wave energy as discussed in the previous section. Interdaily variability in diel ΔpH and ΔDO observed throughout the time series was strongly controlled by changes in light intensity and flow speed, with the decrease in biogeochemical variability from 17–20 October coinciding with decreasing light intensity, and the greater amount of interdaily variability present from 20 October until the end of the study period occurring during a time of greater flow speed fluctuations. During the first week of the study, PAR intensity and flow speed were more consistent, resulting in steadier interdaily biogeochemical variability (Figure 2).

The increased magnitude of daytime increases and nighttime decreases in pH and DO at lower mean flow speeds (high inverse mean flow speeds ($\overline{u^{-1}}$); Figures 5 and 6) observed at almost all sites were consistent with expectations. At low flow speeds, seawater transit times across the reef are longer, and more time is available for metabolic processes to modify the seawater chemistry. Similarly, the increased magnitudes of daytime changes in pH and DO observed with increasing mean PAR were consistent with enhanced rates of primary production under higher light intensities (Cohen et al., 2016; Sawall & Hochberg, 2018).

The magnitude of pH and DO changes at each site were larger during the day than at night. Two-sample *t*-tests performed at each site indicated that mean flow speed did not differ significantly between day and night ($p > 0.6$, Table S4 in Supporting Information S1) suggesting that mean primary production rates during the day were greater than mean respiration rates at night and the Onna-son reef system was net autotrophic throughout the study period. Although calcification and $CaCO_3$ dissolution also affect seawater pH, they do not directly affect DO concentrations, and rates and variability of organic carbon cycling on reefs are typically greater than rates and variability of net community calcification over the diel timescales considered in this study (Cyronak et al., 2018; Pezner et al., 2021; Takeshita et al., 2018).

ΔpH and ΔDO at each site could be influenced by the different benthic communities that water intersects with before reaching each site. The reef flat was primarily composed of a well consolidated pavement covered by crustose coralline algae, rubble, turf algae, and some small coral colonies. In contrast, the lagoon contained scattered patch reefs and areas of macroalgae in addition to sand and rubble, while the channel benthos was primarily sand with scattered coral heads. Depending on the trajectories that different water parcels follow through the reef system, it is possible that they could spend the same time within the reef but be exposed to different benthic communities with different metabolic rates (Jokiel et al., 2014; Page et al., 2016, 2019) and so develop different biogeochemical signals. The consistency of the flow paths observed during this study suggest that this is unlikely to be a notable source of variability during months when wave driven flows dominate, however it may be increasingly important during months with little wave forcing and more variable flows.

Given the observed flow paths of seawater flowing from the reef crest to the lagoon to the channel, we anticipated an increasing signal in ΔpH and ΔDO along this flow path due to the accumulation of biogeochemical modifications. Although the expected trend was indeed observed between the reef crest (C1) and the lagoon (C2), the channel (C3) ΔpH_{day} did not follow this trend as smaller increases in ΔpH_{day} were observed in the channel than in the lagoon. The behavior of nighttime channel pH variability also differed from other sites, as this was the only location where there was no significant correlation between flow speed and pH variability. In contrast, the channel DO variability adhered to the expected downstream trend, and strong relationships were observed between the measured physical drivers and channel diel DO variability. This decoupling of pH and DO may suggest that $CaCO_3$ cycling played a larger role in the channel than on the reef crest or within the lagoon. Daytime pH increases could be suppressed through the consumption of alkalinity by calcification, while the production of alkalinity through $CaCO_3$ dissolution could buffer nighttime pH decreases owing to respiration (Cyronak et al., 2020; Page et al., 2019). Neither of these processes would directly affect the DO concentration.

The benthos of the channel was primarily comprised of fine-grained carbonate sediments susceptible to dissolution, but there were few conspicuous calcifiers beyond the coral heads the sensors were attached to and calcifying foraminifera in the sediments. It is unclear whether this composition of calcifiers could account for the decoupling

of pH and DO variability observed at the benthos in the channel during the day although nighttime dissolution seems like a plausible possibility that has been documented elsewhere (e.g., Page et al., 2016). Another option is that the decoupling of pH and DO in the channel does not represent local changes, but rather is a result of mixing of different water masses. While channel flows did reverse on 17, 21, 22, 23, 26, and 28 October, ΔpH and ΔDO for these days and nights (blue points, Figure 6f) mostly followed the expected trends, with a few notable exceptions and did not account for the variability observed in the channel ΔpH_{night}. Multilayer flow was not observed.

Another aspect to consider in our assessment of daily pH and DO variability is the influence of temperature on chemical equilibria and metabolic rates. Thermodynamic pH variability driven by daily temperature variability was estimated to be approximately ~0.01 units during the day and <0.007 units at night across all sites based on calculations with CO2SYS (Lewis et al., 1998). Assuming a Q_{10} value of 2 (Clausen & Roth, 1975; Edmunds, 2005, 2008; Howe & Marshall, 2001; Scheufen et al., 2017), the mean change in metabolic rates caused by temperature variability was 3.0% on the reef flat, 4.6% in the lagoon, and 5.4% in the channel, while nocturnal variability would produce changes ≤3.0% across all sites. Given the range of ΔpH and ΔDO values observed during this study it is unlikely that temperature changes drive a significant amount of the variability we measured during this study.

5.3. Interactive Effects of PAR and Current Speed on Biogeochemical Variability

The interaction terms present in the lagoon pH and channel DO MLRs were consistent with the expected synergy between flow speed, light intensity, and biogeochemical changes. The degree to which water is modified by metabolic processes is proportional to the product of the rate of the metabolic process and the time the water has been in contact with the metabolizing organisms (i.e., ΔDO or $\Delta pH \propto \text{rate} \times \text{time}$). Consequently, at low flow speeds water will spend more time in the reef system and so be exposed to PAR-enhanced metabolic rates (e.g., Chalker et al., 1975; Cohen et al., 2016) for longer, resulting in a greater biogeochemical change. The effect of PAR on ΔDO and ΔpH is therefore dependent on the flow speed, with this dependence appearing as an interactive term in the MLRs. The lack of significant interaction terms in the MLRs for reef flat ΔpH_{day} and ΔDO_{day} with high leverage points removed was unexpected and may reflect the increased difficulty of resolving significant interactions within smaller signals, while the absence of interaction terms in the lagoon ΔDO_{day} MLR and channel ΔpH_{day} MLR may stem from the small sample size resulting from biofouling (lagoon DO_{day}) and the mechanisms responsible for decoupling pH and DO previously discussed (channel ΔpH_{day}).

pH and DO variability not explained by the MLR models may stem from several non-linearities present within the system. Slow flow speeds can cause mass transfer limitation and subsequently decrease metabolic rates, while high flow speeds can enhance metabolic rates by alleviating mass transfer limitation (Baird et al., 2004; Edmunds & Burgess, 2017; Falter et al., 2004; Mass et al., 2010), with either of these processes resulting in the relationship between flow speed and ΔpH or ΔDO becoming nonlinear. Additionally, coral photosynthesis-irradiance (PI) curves are non-linear (Anthony & Hoegh-Guldberg, 2003; Mass et al., 2007; Rodolfo-Metalpa et al., 2008), with the photosynthetic rate achieving a maximum value beyond a certain light intensity, though Sawall and Hochberg (2018) found PI relations tended to be linear over daily or longer timescales. Quicker light saturation of calcifying and photosynthetic organisms on the shallow reef flat may explain the lack of an interaction term observed in reef flat ΔpH_{day} and ΔDO_{day} MLRs, while the presence of interaction terms in the deeper lagoon may indicate that photo-saturation does not occur to the same degree. Differences in how these phenomena affect each site could also result from differences in community composition, as different organisms experience mass-transfer limitation at different thresholds (Falter et al., 2004; Reidenbach et al., 2006) and PI curves vary between species (Sawall & Hochberg, 2018 and references therein). The logarithmic nature of the pH scale and the series of chemical equilibria that regulate carbonate chemistry are additional complicating factors that may produce variability that was not captured by the MLR models and explain why correlations between flow speed, PAR, and ΔDO were typically stronger than those between the physical drivers and ΔpH.

5.4. Implications

Physical controls of biogeochemical and physical variability may influence the susceptibility of different coral reefs and coral reef habitats to future anthropogenic climate change in multiple and contrasting ways. On coral reefs with high flow speeds and short residence times, water may not stay within the reef system long enough to

develop a large biogeochemical signal and so extreme pH and DO values may not occur as early or as frequently as they would on reefs with slow flow speeds and high residence times. High flow speeds also reduce the thickness of diffusive and thermal boundary layers (Mass et al., 2010), potentially increasing coral resilience by increasing gas exchange, nutrient uptake (Baird et al., 2004; Falter et al., 2004, 2005), waste removal, thermal dissipation (Jimenez et al., 2011; Rowan et al., 1997), and enhancing coral autotrophy (Mass et al., 2010; Osinga et al., 2017), growth (Schutter et al., 2010, 2011), and heterotrophy (at least up to speeds beyond which tentacular feeding is suppressed; Wijgerde et al., 2012). Conversely, while reef regions that experience high levels of physical and biogeochemical variability may cross physiological thresholds sooner, there are indications that corals exposed to large biogeochemical and physical variability are more resistant to the stresses imposed by ocean warming and acidification (Cornwall et al., 2018; Rivest et al., 2017; Schoepf et al., 2015). Additionally, rising sea levels and changes in coral reef structure may alter coral reef circulation, and corals that currently benefit from high flow speeds may be particularly susceptible to these changes if the flow speeds they experience are reduced. Determining the effects of physical factors such as flow speed and light intensity on coral resilience is vital for predicting how reefs will fare in the future under warmer, less oxygenated, and more acidic conditions.

In addition to bettering our understanding of the drivers of pH and DO variability, constraining the circulation of coral reefs may aid future management efforts (Rivest et al., 2017), including within the Onna reef system. The uptake of carbon by seaweed farms near coral reefs may alleviate local ocean acidification (Mongin et al., 2016; Unsworth et al., 2012), however this method requires corals be located downstream of the seaweed farms. The consistency of the seawater flow paths observed during this study and the existence of Mozuku seaweed farms make the Onna-son reef system an ideal location to further investigate this hypothesis.

The observed physical control of biogeochemical variability and the highly consistent nature of the flow during this study also raises the possibility that biogeochemical variability may be predictable if the seawater circulation and incident PAR of a coral reef system is known (Cyronak et al., 2020). Employing recent advances in remote sensing techniques and hydrodynamic models to develop such predictive capacity would further improve our ability to identify corals growing in high and low variance regions and predict how future ocean changes will impact individual reef environments (Foo & Asner, 2019).

The effects of flow speed and light intensity on pH and DO variability extend to other parameters that are predominantly altered by benthic metabolic processes, such as total alkalinity (TA) or dissolved inorganic carbon (DIC). Changes in TA and DIC throughout a reef system are often used to calculate reef metabolism and assess coral reef function. While uncertainties in flow speed are recognized as one of the greatest sources of error in reef metabolism calculations (Courtney & Andersson, 2019), our results highlight the role light intensity plays in determining biogeochemical variability (Barnes & Devereux, 1984). As field campaigns are often relatively short, the effect of several uncommonly sunny or cloudy days could result in large variations in metabolic rates measured within the same reef.

6. Conclusions

Despite the mean tidal range to significant wave height ratio being above one throughout the study period, flow speed and direction within the coral reef system in Onna-son, Japan, was predominantly driven by waves, but modulated by tides. In the context of annual significant wave height patterns for Okinawa, it is likely that circulation in Onna-son is primarily wave driven from October through January but may be tidally driven during the summer months. Reef circulation was highly consistent throughout the study period and followed benthic striations visible from satellite imagery. PAR intensity during this study was likely moderate to low compared to annual values. Together, PAR intensity and flow speed explained 25%–74% of the daytime pH and DO variability and 7%–75% of the nighttime variability in these parameters across a reef flat, lagoon, and outflow channel within the study area. The relative importance of these drivers is likely to vary seasonally, with the influence of flow speed increasing during the winter months characterized by larger waves and lower PAR intensities, and PAR becoming more significant during summer when the waves are smaller and the days are longer. Variability for both pH and DO generally increased from the reef flat to the lagoon and the channel as a result of longer transit times and the accumulation of signals from different reef environments as seawater moved from the reef flat to the channel. Light intensity and flow speed explained a large proportion of the DO variability observed in the channel (68% during the day, 75% at night), but little of the pH variability (25% during the day and 7% at night), suggesting that the drivers of variability for these parameters may be decoupled at this site.

Our results demonstrate the critical role physical drivers play in controlling coral reef biogeochemical variability. The strong influence of physical factors on biogeochemical variability, and the highly consistent nature of the reef circulation observed also indicate that on certain reefs it may be possible to predict biogeochemical variability by constraining their circulation and incident PAR. Identifying the reef characteristics that would allow biogeochemical variability to be predicted from physical measurements warrants future study.

Data Availability Statement

The data set analyzed in this study is available at https://doi.org/10.5061/dryad.gf1vhhmrc.

Acknowledgments
We would like to thank Kazumi Inoha, Captain Kazuya Hayashi, Yoshimi Higa, Tomoko Yoshino, Yuna Zayasu, and the Onna Village Fisheries Cooperative for their invaluable assistance. This paper was greatly improved by the thoughtful and constructive comments of two anonymous reviewers, and we thank them for the time and effort they put into their reviews. This research was funded by the UC San Diego Academic Senate Marine Sciences Research Grant A1054379 (AJA) and Belmont Forum/NSF ICER 2029205 (AJA). MSR, TAC, AKP, and JLD were supported by NSF GRFPs.

References

Albright, R., Benthuysen, J., Cantin, N., Caldeira, K., & Anthony, K. (2015). Coral reef metabolism and carbon chemistry dynamics of a coral reef flat. *Geophysical Research Letters*, *42*(10), 3980–3988. https://doi.org/10.1002/2015GL063488

Albright, R., Takeshita, Y., Koweek, D. A., Ninokawa, A., Wolfe, K., Rivlin, T., et al. (2018). Carbon dioxide addition to coral reef waters suppresses net community calcification. *Nature*, *555*(7697), 516–519. https://doi.org/10.1038/nature25968

Altieri, A. H., Harrison, S. B., Seemann, J., Collin, R., Diaz, R. J., & Knowlton, N. (2017). Tropical dead zones and mass mortalities on coral reefs. *Proceedings of the National Academy of Sciences of the United States of America*, *114*(14), 3660–3665. https://doi.org/10.1073/pnas.1621517114

Andersson, A. J., & Gledhill, D. (2013). Ocean acidification and coral reefs: Effects on breakdown, dissolution, and net ecosystem calcification. *Annual Review of Marine Science*, *5*(1), 321–348. https://doi.org/10.1146/annurev-marine-121211-172241

Anthony, K. R., & Hoegh-Guldberg, O. (2003). Kinetics of photoacclimation in corals. *Oecologia*, *134*(1), 23–31. https://doi.org/10.1007/s00442-002-1095-1

Anthony, K. R. N., Kline, D. I., Diaz-Pulido, G., Dove, S., & Hoegh-Guldberg, O. (2008). Ocean acidification causes bleaching and productivity loss in coral reef builders. *Proceedings of the National Academy of Sciences of the United States of America*, *105*(45), 17442–17446. https://doi.org/10.1073/pnas.0804478105

Baird, M. E., Roughan, M., Brander, R. W., Middleton, J. H., & Nippard, G. J. (2004). Mass-transfer-limited nitrate uptake on a coral reef flat, Warraber Island, Torres Strait, Australia. *Coral Reefs*, *23*(3), 386–396. https://doi.org/10.1007/s00338-004-0404-z

Barnes, D. J., & Devereux, M. J. (1984). Productivity and calcification on a coral reef: A survey using pH and oxygen electrode techniques. *Journal of Experimental Marine Biology and Ecology*, *79*(3), 213–231. https://doi.org/10.1016/0022-0981(84)90196-5

Breitburg, D., Levin, L. A., Oschlies, A., Grégoire, M., Chavez, F. P., Conley, D. J., et al. (2018). Declining oxygen in the global ocean and coastal waters. *Science*, *359*(6371), eaam7240. https://doi.org/10.1126/science.aam7240

Bresnahan, P. J., Martz, T. R., Takeshita, Y., Johnson, K. S., & LaShomb, M. (2014). Best practices for autonomous measurement of seawater pH with the Honeywell Durafet. *Methods in Oceanography*, *9*, 44–60. https://doi.org/10.1016/j.mio.2014.08.003

Bruno, J. F., & Selig, E. R. (2007). Regional decline of coral cover in the Indo-Pacific: Timing, extent, and subregional comparisons. *PLoS One*, *2*(8), e711. https://doi.org/10.1371/journal.pone.0000711

Chalker, B. E., Taylor, D. L., & Yonge, M. (1975). Light-enhanced calcification, and the role of oxidative phosphorylation in calcification of the coral *Acropora Cervicornis*. *Proceedings of the Royal Society of London. Series B. Biological Sciences*, *190*(1100), 323–331. https://doi.org/10.1098/rspb.1975.0096

Clausen, C. D., & Roth, A. A. (1975). Effect of temperature and temperature adaptation on calcification rate in the Hermatypic coral *Pocillopora damicomis*. *Marine Biology*, *33*(2), 93–100. https://doi.org/10.1007/bf00390713

Cohen, I., Dubinsky, Z., & Erez, J. (2016). Light enhanced calcification in hermatypic corals: New Insights from light spectral responses. *Frontiers in Marine Science*, *2*, 122. https://doi.org/10.3389/fmars.2015.00122

Comeau, S., Edmunds, P. J., Lantz, C. A., & Carpenter, R. C. (2014). Water flow modulates the response of coral reef communities to ocean acidification. *Scientific Reports*, *4*(1), 6681. https://doi.org/10.1038/srep06681

Cornwall, C. E., Comeau, S., DeCarlo, T. M., Moore, B., D'Alexis, Q., & McCulloch, M. T. (2018). Resistance of corals and coralline algae to ocean acidification: Physiological control of calcification under natural pH variability. *Proceedings of the Royal Society B: Biological Sciences*, *285*(1884), 20181168. https://doi.org/10.1098/rspb.2018.1168

Courtney, T. A., & Andersson, A. J. (2019). Evaluating measurements of coral reef net ecosystem calcification rates. *Coral Reefs*, *42*(3), 1–10. https://doi.org/10.1007/s00338-019-01828-2

Cyronak, T., Andersson, A. J., Langdon, C., Albright, R., Bates, N. R., Caldeira, K., et al. (2018). Taking the metabolic pulse of the world's coral reefs. *PLoS One*, *13*(1), e0190872. https://doi.org/10.1371/journal.pone.0190872

Cyronak, T., Santos, I. R., & Eyre, B. D. (2013). Permeable coral reef sediment dissolution driven by elevated pCO_2 and pore water advection. *Geophysical Research Letters*, *40*(18), 4876–4881. https://doi.org/10.1002/grl.50948

Cyronak, T., Takeshita, Y., Courtney, T. A., DeCarlo, E. H., Eyre, B. D., Kline, D. I., et al. (2020). Diel temperature and pH variability scale with depth across diverse coral reef habitats. *Limnology and Oceanography Letters*, *5*(2), 193–203. https://doi.org/10.1002/lol2.10129

Darling, E. S., McClanahan, T. R., Maina, J., Gurney, G. G., Graham, N. A. J., Januchowski-Hartley, F., et al. (2019). Social–environmental drivers inform strategic management of coral reefs in the Anthropocene. *Nature Ecology & Evolution*, *3*(9), 1341–1350. https://doi.org/10.1038/s41559-019-0953-8

Davis, K. L., McMahon, A., Correa, R. E., & Santos, I. R. (2020). Calcification and organic productivity at the world's southernmost coral reef. *Marine Chemistry*, *227*, 103870. https://doi.org/10.1016/j.marchem.2020.103870

DeCarlo, T. M., Cohen, A. L., Wong, G. T. F., Davis, K. A., Lohmann, P., & Soong, K. (2017). Mass coral mortality under local amplification of 2°C ocean warming. *Scientific Reports*, *7*(1), 44586. https://doi.org/10.1038/srep44586

Dennison, W. C., & Barnes, D. J. (1988). Effect of water motion on coral photosynthesis and calcification. *Journal of Experimental Marine Biology and Ecology*, *115*(1), 67–77. https://doi.org/10.1016/0022-0981(88)90190-6

Diaz, R. J., & Rosenberg, R. (2008). Spreading dead zones and consequences for marine ecosystems. *Science*, *321*(5891), 926–929. https://doi.org/10.1126/science.1156401

Domingues, C. M., Church, J. A., White, N. J., Gleckler, P. J., Wijffels, S. E., Barker, P. M., & Dunn, J. R. (2008). Improved estimates of upper-ocean warming and multi-decadal sea-level rise. *Nature*, *453*(7198), 1090–1093. https://doi.org/10.1038/nature07080

Doney, S. C., Busch, D. S., Cooley, S. R., & Kroeker, K. J. (2020). The impacts of ocean acidification on marine ecosystems and reliant human communities. *Annual Review of Environment and Resources*, *45*(1), 83–112. https://doi.org/10.1146/annurev-environ-012320-083019

Doney, S. C., Fabry, V. J., Feely, R. A., & Kleypas, J. A. (2009). Ocean acidification: The other CO_2 problem. *Annual Review of Marine Science*, *1*(1), 169–192. https://doi.org/10.1146/annurev.marine.010908.163834

Dove, S. G., Brown, K. T., Van Den Heuvel, A., Chai, A., & Hoegh-Guldberg, O. (2020). Ocean warming and acidification uncouple calcification from calcifier biomass which accelerates coral reef decline. *Communications Earth & Environment*, *1*(1), 1–9. https://doi.org/10.1038/s43247-020-00054-x

Dove, S. G., Kline, D. I., Pantos, O., Angly, F. E., Tyson, G. W., & Hoegh-Guldberg, O. (2013). Future reef decalcification under a business-as-usual CO_2 emission scenario. *Proceedings of the National Academy of Sciences of the United States of America*, *110*(38), 15342–15347. https://doi.org/10.1073/pnas.1302701110

Dumas, F., Le Gendre, R., Thomas, Y., & Andréfout, S. (2012). Tidal flushing and wind driven circulation of Ahe atoll lagoon (Tuamotu Archipelago, French Polynesia) from in situ observations and numerical modelling. *Marine Pollution Bulletin*, *65*(10–12), 425–440. https://doi.org/10.1016/j.marpolbul.2012.05.041

Durack, P. J., Gleckler, P. J., Purkey, S. G., Johnson, G. C., Lyman, J. M., & Boyer, T. P. (2018). Ocean warming: From the surface to the deep in observations and models. *Oceanography*, *31*(2), 41–51. https://doi.org/10.2307/26542650

Edmunds, P. J. (2005). Effect of elevated temperature on aerobic respiration of coral recruits. *Marine Biology*, *146*(4), 655–663. https://doi.org/10.1007/s00227-004-1485-5

Edmunds, P. J. (2008). Differential effects of high temperature on the respiration of juvenile Caribbean Corals. *Bulletin of Marine Science*, *83*(3), 453–464.

Edmunds, P. J., & Burgess, S. C. (2017). Colony size and turbulent flow speed modulate the calcification response of the coral Pocillopora verrucosa to temperature. *Marine Biology*, *165*(13), 13. https://doi.org/10.1007/s00227-017-3257-z

Eyre, B. D., Cyronak, T., Drupp, P., De Carlo, E. H., Sachs, J. P., & Andersson, A. J. (2018). Coral reefs will transition to net dissolving before end of century. *Science*, *359*(6378), 908–911. https://doi.org/10.1126/science.aao1118

Fabricius, K. E., Langdon, C., Uthicke, S., Humphrey, C., Noonan, S., De'ath, G., et al. (2011). Losers and winners in coral reefs acclimatized to elevated carbon dioxide concentrations. *Nature Climate Change*, *1*(3), 165–169. https://doi.org/10.1038/nclimate1122

Falter, J. L., Atkinson, M. J., & Coimbra, C. F. M. (2005). Effects of surface roughness and oscillatory flow on the dissolution of plaster forms: Evidence for nutrient mass transfer to coral reef communities. *Limnology & Oceanography*, *50*(1), 246–254. https://doi.org/10.4319/lo.2005.50.1.0246

Falter, J. L., Atkinson, M. J., & Merrifield, M. A. (2004). Mass-transfer limitation of nutrient uptake by a wave-dominated reef flat community. *Limnology & Oceanography*, *49*(5), 1820–1831. https://doi.org/10.4319/lo.2004.49.5.1820

Falter, J. L., Lowe, R. J., Zhang, Z., & McCulloch, M. (2013). Physical and biological controls on the carbonate chemistry of coral reef waters: Effects of metabolism, wave forcing, sea level, and geomorphology. *PLoS One*, *8*(1), e53303. https://doi.org/10.1371/journal.pone.0053303

Foo, S. A., & Asner, G. P. (2019). Scaling up coral reef restoration using remote sensing technology. *Frontiers in Marine Science*, *6*, e81478. https://doi.org/10.3389/fmars.2019.00079

Gardner, T. A., Côté, I. M., Gill, J. A., Grant, A., & Watkinson, A. R. (2003). Long-term region-wide declines in Caribbean corals. *Science*, *301*(5635), 958–960. https://doi.org/10.1126/science.1086050

Gattuso, J. P., Pichon, M., Delesalle, B., Canon, C., & Frankignoulle, M. (1996). Carbon fluxes in coral reefs. I. Lagrangian measurement of community metabolism and resulting air-sea CO_2 disequilibrium. *Marine Ecology Progress Series*, *145*, 109–121. https://doi.org/10.3354/meps145109

Gattuso, J. P., Pichon, M., Delesalle, B., & Frankignoulle, M. (1993). Community metabolism and air-sea CO_2 fluxes in a coral reef ecosystem (Moorea, French Polynesia). *Marine Ecology Progress Series*, *96*, 259–267. https://doi.org/10.3354/meps096259

Glynn, P. W., & Manzello, D. P. (2015). Bioerosion and coral reef growth: A dynamic balance. In C. Birkeland (Ed.), *Coral reefs in the Anthropocene*. Springer. https://doi.org/10.1007/978-94-017-7249-5_4

Godin, G. (1972). *The analysis of tides*. University of Toronto Press.

Grossmann, M. M., Gallager, S. M., & Mitarai, S. (2015). Continuous monitoring of near-bottom mesoplankton communities in the East China Sea during a series of typhoons. *Journal of Oceanography*, *71*(1), 115–124. https://doi.org/10.1007/s10872-014-0268-y

Gruber, R. K., Lowe, R. J., & Falter, J. L. (2017). Metabolism of a tide-dominated reef platform subject to extreme diel temperature and oxygen variations. *Limnology & Oceanography*, *62*(4), 1701–1717. https://doi.org/10.1002/lno.10527

Guadayol, Ò., Silbiger, N. J., Donahue, M. J., & Thomas, F. I. M. (2014). Patterns in temporal variability of temperature, oxygen and pH along an environmental gradient in a coral reef. *PLoS One*, *9*(1), e85213. https://doi.org/10.1371/journal.pone.0085213

Guan, Y., Hohn, S., Wild, C., & Merico, A. (2020). Vulnerability of global coral reef habitat suitability to ocean warming, acidification and eutrophication. *Global Change Biology*, *26*(10), 5646–5660. https://doi.org/10.1111/gcb.15293

Guo, W., Bokade, R., Cohen, A. L., Mollica, N. R., Leung, M., & Brainard, R. E. (2020). Ocean acidification has impacted coral growth on the great barrier reef. *Geophysical Research Letters*, *47*(19), e2019GL086761. https://doi.org/10.1029/2019GL086761

Hann, J. (1903). *Handbook of climatology*. The MacMillan Company.

Hobbs, J. P. A., & McDonald, C. A. (2010). Increased seawater temperature and decreased dissolved oxygen triggers fish kill at the Cocos (Keeling) Islands, Indian Ocean. *Journal of Fish Biology*, *77*(6), 1219–1229. https://doi.org/10.1111/j.1095-8649.2010.02726.x

Hoegh-Guldberg, O., Mumby, P. J., Hooten, A. J., Steneck, R. S., Greenfield, P., Gomez, E., et al. (2007). Coral reefs under rapid climate change and ocean acidification. *Science*, *318*(5857), 1737–1742. https://doi.org/10.1126/science.1152509

Howe, S. A., & Marshall, A. T. (2001). Thermal compensation of metabolism in the temperate coral, Plesiastrea versipora (Lamarck, 1816). *Journal of Experimental Marine Biology and Ecology*, *259*(2), 231–248. https://doi.org/10.1016/S0022-0981(01)00230-1

Hughes, T. P., Baird, A. H., Bellwood, D. R., Card, M., Connolly, S. R., Folke, C., et al. (2003). Climate change, human impacts, and the resilience of coral reefs. *Science*, *301*(5635), 929–933. https://doi.org/10.1126/science.1085046

Hughes, T. P., Kerry, J. T., Alvarez-Noriega, M., Alvarez-Romero, J. G., Anderson, K. D., Baird, A. H., et al. (2017). Global warming and recurrent mass bleaching of corals. *Nature*, *543*(7645), 373–377. https://doi.org/10.1038/nature21707

Jackson, E. J., Donovan, M., Cramer, K., & Lam, V. (2014). *Status and trends of Caribbean coral reefs: 1970–2012*. Global Coral Reef Monitoring Network, IUCN.

Jimenez, I. M., Kühl, M., Larkum, A. W. D., & Ralph, P. J. (2011). Effects of flow and colony morphology on the thermal boundary layer of corals. *Journal of the Royal Society Interface*, *8*(65), 1785–1795. https://doi.org/10.1098/rsif.2011.0144

Jokiel, P. L., Jury, C. P., & Rodgers, K. S. (2014). Coral-algae metabolism and diurnal changes in the CO_2-carbonate system of bulk sea water. *PeerJ*, *2*, e378. https://doi.org/10.7717/peerj.378

Kealoha, A. K., Doyle, S. M., Shamberger, K. E. F., Sylvan, J. B., Hetland, R. D., & DiMarco, S. F. (2020). Localized hypoxia may have caused coral reef mortality at the Flower Garden Banks. *Coral Reefs*, *39*(1), 119–132. https://doi.org/10.1007/s00338-019-01883-9

Keeling, R. F., Körtzinger, A., & Gruber, N. (2009). Ocean deoxygenation in a warming world. *Annual Review of Marine Science*, *2*(1), 199–299. https://doi.org/10.1146/annurev.marine.010908.163855

Kekuewa, S. A. H., Courtney, T. A., Cyronak, T., Kindeberg, T., Eyre, B. D., Stoltenberg, L., & Andersson, A. J. (2021). Temporal and spatial variability of chemical and physical parameters on the Heron Island coral reef platform. *Aquatic Geochemistry*, *27*(4), 241–268. https://doi.org/10.1007/s10498-021-09400-7

Kinsey, D. W. (1978). Productivity and calcification estimates using slack-water periods and field enclosures. *Coral Reefs: Research Methods*, 439–468.

Kinsey, D. W. (1985). Metabolism, calcification and production: I systems level studies. In *Proceedings of the Fifth International Coral Reef Congress* (Vol. *4*, 503–542).

Kleypas, J. A., Buddemeier, R. W., Archer, D., Gattuso, J. P., Langdon, C., & Opdyke, B. N. (1999). Geochemical consequences of increased atmospheric carbon dioxide on coral reefs. *Science*, *284*(5411), 118–120. https://doi.org/10.1126/science.284.5411.118

Koweek, D. A., Dunbar, R. B., Monismith, S. G., Mucciarone, D. A., Woodson, C. B., & Samuel, L. (2015). High-resolution physical and biogeochemical variability from a shallow back reef on Ofu, American Samoa: An end-member perspective. *Coral Reefs*, *34*(3), 979–991. https://doi.org/10.1007/s00338-015-1308-9

Kraines, S. B., Suzuki, A., Yanagi, T., Isobe, M., Guo, X., & Komiyama, H. (1999). Rapid water exchange between the lagoon and the open ocean at Majuro Atoll due to wind, waves, and tide. *Journal of Geophysical Research*, *104*(C7), 15635–15653. https://doi.org/10.1029/1999JC900065

Kwiatkowski, L., & Orr, J. C. (2018). Diverging seasonal extremes for ocean acidification during the twenty-first century. *Nature Climate Change*, *8*(2), 141–145. https://doi.org/10.1038/s41558-017-0054-0

Lee, I.-H., Fan, T.-Y., Fu, K.-H., & Ko, D. S. (2020). Temporal variation in daily temperature minima in coral reefs of Nanwan Bay, Southern Taiwan. *Scientific Reports*, *10*(1), 8656. https://doi.org/10.1038/s41598-020-65194-8

Lentz, S. J., Churchill, J. H., Davis, K. A., Farrar, J. T., Pineda, J., & Starczak, V. (2016). The characteristics and dynamics of wave-driven flow across a platform coral reef in the Red Sea. *Journal of Geophysical Research: Oceans*, *121*(2), 1360–1376. https://doi.org/10.1002/2015JC011141

Levitus, S., Antonov, J., & Boyer, T. (2005). Warming of the world ocean, 1955–2003. *Geophysical Research Letters*, *32*(2), L02604. https://doi.org/10.1029/2004GL021592

Lewis, E., Wallace, D., & Allison, L. J. (1998). *Program developed for CO_2 system calculations (No. ORNL/CDIAC-105)*. Brookhaven National Laboratory, Department of Applied Science, Upton, NY (United States), Oak Ridge National Laboratory, Carbon Dioxide Information Analysis Center, TN (United States). https://doi.org/10.2172/639712

Li, J., Knapp, D. E., Lyons, M., Roelfsema, C., Phinn, S., Schill, S. R., & Asner, G. P. (2021). Automated global shallow water bathymetry mapping using Google Earth engine. *Remote Sensing*, *13*(8), 1469. https://doi.org/10.3390/rs13081469

Lindhart, M., Rogers, J. S., Maticka, S. A., Woodson, C. B., & Monismith, S. G. (2021). Wave modulation of flows on open and closed reefs. *Journal of Geophysical Research: Oceans*, *126*(4), e2020JC016645. https://doi.org/10.1029/2020JC016645

Longuet-Higgins, M. S., & Stewart, R. W. (1962). Radiation stress and mass transport in gravity waves, with application to 'surf beats'. *Journal of Fluid Mechanics*, *13*(4), 481–504. https://doi.org/10.1017/S0022112062000877

Lowe, R. J., & Falter, J. L. (2015). Oceanic forcing of coral reefs. *Annual Review of Marine Science*, *7*(1), 43–66. https://doi.org/10.1146/annurev-marine-010814-015834

Lowe, R. J., Falter, J. L., Monismith, S. G., & Atkinson, M. J. (2009a). A numerical study of circulation in a coastal reef-lagoon system. *Journal of Geophysical Research*, *114*(C6), C06022. https://doi.org/10.1029/2008JC005081

Lowe, R. J., Falter, J. L., Monismith, S. G., & Atkinson, M. J. (2009b). Wave-driven circulation of a coastal reef–lagoon system. *Journal of Physical Oceanography*, *39*(4), 873–893. https://doi.org/10.1175/2008JPO3958.1

Mass, T., Einbinder, S., Brokovich, E., Shashar, N., Vago, R., Erez, J., & Dubinsky, Z. (2007). Photoacclimation of Stylophora pistillata to light extremes: Metabolism and calcification. *Marine Ecology Progress Series*, *334*, 93–102. https://doi.org/10.3354/meps334093

Mass, T., Genin, A., Shavit, U., Grinstein, M., & Tchernov, D. (2010). Flow enhances photosynthesis in marine benthic autotrophs by increasing the efflux of oxygen from the organism to the water. *Proceedings of the National Academy of Sciences*, *107*(6), 2527–2531. https://doi.org/10.1073/pnas.0912348107

McClanahan, T. R., Donner, S. D., Maynard, J. A., MacNeil, M. A., Graham, N. A. J., Maina, J., et al. (2012). Prioritizing key resilience indicators to support coral reef management in a changing climate. *PLoS One*, *7*(8), e42884. https://doi.org/10.1371/journal.pone.0042884

Mongin, M., & Baird, M. E. (2014). The interacting effects of photosynthesis, calcification and water circulation on carbon chemistry variability on a coral reef flat: A modelling study. *Ecological Modelling*, *284*, 19–34. https://doi.org/10.1016/j.ecolmodel.2014.04.004

Mongin, M., Baird, M. E., Hadley, S., & Lenton, A. (2016). Optimising reef-scale CO_2 removal by seaweed to buffer ocean acidification. *Environmental Research Letters*, *11*(3), 034023. https://doi.org/10.1088/1748-9326/11/3/034023

Monismith, S. G. (2007). Hydrodynamics of coral reefs. *Annual Review of Fluid Mechanics*, *39*(1), 37–55. https://doi.org/10.1146/annurev.fluid.38.050304.092125

Monismith, S. G., Ahmerkamp, S., Hench, J. L., Herdman, L. M. M., & Ahmerkamp, S. (2013). Wave transformation and wave-driven flow across a steep coral reef. *Journal of Physical Oceanography*, *43*(7), 1356–1379. https://doi.org/10.1175/JPO-D-12-0164.1

Munk, W. H., & Sargent, M. C. (1948). Adjustment of bikini atoll to ocean waves. *Eos, Transactions American Geophysical Union*, *29*(6), 855–860. https://doi.org/10.1029/TR029i006p00855

Osinga, R., Derksen-Hooijberg, M., Wijgerde, T., & Verreth, J. A. J. (2017). Interactive effects of oxygen, carbon dioxide and flow on photosynthesis and respiration in the scleractinian coral *Galaxea fascicularis*. *Journal of Experimental Biology*, *220*(12), 2236–2242. https://doi.org/10.1242/jeb.140509

Page, H. N., Andersson, A. J., Jokiel, P. L., Rodgers, K. S., Lebrato, M., Yeakel, K., et al. (2016). Differential modification of seawater carbonate chemistry by major coral reef benthic communities. *Coral Reefs*, *35*(4), 1311–1325. https://doi.org/10.1007/s00338-016-1490-4

Page, H. N., Courtney, T. A., De Carlo, E. H., Howins, N. M., Koester, I., & Andersson, A. J. (2019). Spatiotemporal variability in seawater carbon chemistry for a coral reef flat in Kāne'ohe Bay, Hawai'i. *Limnology & Oceanography*, *64*(3), 913–934. https://doi.org/10.1002/lno.11084

Pezner, A. K., Courtney, T. A., Page, H. N., Giddings, S. N., Beatty, C. M., DeGrandpre, M. D., & Andersson, A. J. (2021). Lateral, vertical, and temporal variability of seawater carbonate chemistry at Hog reef, Bermuda. *Frontiers in Marine Science*, *8*, 562267. https://doi.org/10.3389/fmars.2021.562267

Price, N. N., Martz, T. R., Brainard, R. E., & Smith, J. E. (2012). Diel variability in seawater pH relates to calcification and benthic community structure on coral reefs. *PLoS One*, *7*(8), e43843. https://doi.org/10.1371/journal.pone.0043843

Raj, K. D., Mathews, G., Obura, D. O., Laju, R. L., Bharath, M. S., Kumar, P. D., et al. (2020). Low oxygen levels caused by Noctiluca scintillans bloom kills corals in Gulf of Mannar, India. *Scientific Reports*, *10*(1), 1–7. https://doi.org/10.1038/s41598-020-79152-x

Reid, E. C., Lentz, S. J., DeCarlo, T. M., Cohen, A. L., & Davis, K. A. (2020). Physical processes determine spatial structure in water temperature and residence time on a wide reef flat. *Journal of Geophysical Research: Oceans*, *125*(12), e2020JC016543. https://doi.org/10.1029/2020JC016543

Reidenbach, M. A., Koseff, J. R., Monismith, S. G., Steinbuckc, J. V., & Genin, A. (2006). The effects of waves and morphology on mass transfer within branched reef corals. *Limnology & Oceanography*, *51*(2), 1134–1141. https://doi.org/10.4319/lo.2006.51.2.1134

Rivest, E. B., Comeau, S., & Cornwall, C. E. (2017). The role of natural variability in shaping the response of coral reef organisms to climate change. *Current Climate Change Reports*, *3*(4), 271–281. https://doi.org/10.1007/s40641-017-0082-x

Rodolfo-Metalpa, R., Huot, Y., & Ferrier-Pagès, C. (2008). Photosynthetic response of the Mediterranean zooxanthellate coral *Cladocora caespitosa* to the natural range of light and temperature. *Journal of Experimental Biology*, *211*(10), 1579–1586. https://doi.org/10.1242/jeb.016345

Rogers, J. S., Monismith, S. G., Koweek, D. A., Torres, W. I., & Dunbar, R. B. (2016). Thermodynamics and hydrodynamics in an atoll reef system and their influence on coral cover. *Limnology & Oceanography*, *61*(6), 2191–2206. https://doi.org/10.1002/lno.10365

Rowan, R., Knowlton, N., Baker, A., & Jara, J. (1997). Landscape ecology of algal symbionts creates variation in episodes of coral bleaching. *Nature*, *388*(6639), 265–269. https://doi.org/10.1038/40843

Ruiz-Moreno, D., Willis, B. L., Page, A. C., Weil, E., Cróquer, A., Vargas-Angel, B., et al. (2012). Global coral disease prevalence associated with sea temperature anomalies and local factors. *Diseases of Aquatic Organisms*, *100*(3), 249–261. https://doi.org/10.3354/dao02488

Safaie, A., Silbiger, N. J., McClanahan, T. R., Pawlak, G., Barshis, D. J., Hench, J. L., et al. (2018). High frequency temperature variability reduces the risk of coral bleaching. *Nature Communications*, *9*(1), 1671. https://doi.org/10.1038/s41467-018-04074-2

Sawall, Y., & Hochberg, E. J. (2018). Diel versus time-integrated (daily) photosynthesis and irradiance relationships of coral reef organisms and communities. *PLoS One*, *13*(12), e0208607. https://doi.org/10.1371/journal.pone.0208607

Scheufen, T., Krämer, W. E., Iglesias-Prieto, R., & Enríquez, S. (2017). Seasonal variation modulates coral sensibility to heat-stress and explains annual changes in coral productivity. *Scientific Reports*, *7*(1), 4937. https://doi.org/10.1038/s41598-017-04927-8

Schoepf, V., Stat, M., Falter, J. L., & McCulloch, M. T. (2015). Limits to the thermal tolerance of corals adapted to a highly fluctuating, naturally extreme temperature environment. *Scientific Reports*, *5*(1), 17639. https://doi.org/10.1038/srep17639

Schutter, M., Crocker, J., Paijmans, A., Janse, M., Osinga, R., Verreth, A. J., & Wijffels, R. H. (2010). The effect of different flow regimes on the growth and metabolic rates of the scleractinian coral *Galaxea fascicularis*. *Coral Reefs*, *29*(3), 737–748. https://doi.org/10.1007/s00338-010-0617-2

Schutter, M., Kranenbarg, S., Wijffels, R. H., Verreth, J., & Osinga, R. (2011). Modification of light utilization for skeletal growth by water flow in the scleractinian coral *Galaxea fascicularis*. *Marine Biology*, *158*(4), 769–777. https://doi.org/10.1007/s00227-010-1605-3

Shaw, E. C., McNeil, B. I., & Tilbrook, B. (2012). Impacts of ocean acidification in naturally variable coral reef flat ecosystems. *Journal of Geophysical Research*, *117*(C3), C03038. https://doi.org/10.1029/2011JC007655

Smale, D. A. (2020). Impacts of ocean warming on kelp forest ecosystems. *New Phytologist*, *225*(4), 1447–1454. https://doi.org/10.1111/nph.16107

Smith, J. E., Price, N. N., Nelson, C. E., & Haas, A. F. (2013). Coupled changes in oxygen concentration and pH caused by metabolism of benthic coral reef organisms. *Marine Biology*, *160*(9), 2437–2447. https://doi.org/10.1007/s00227-013-2239-z

Smith, S. V., & Key, G. S. (1975). Carbon-dioxide and metabolism in marine environments. *Limnology & Oceanography*, *20*(3), 493–495. https://doi.org/10.4319/lo.1975.20.3.0493

Symonds, G., Black, K. P., & Young, I. R. (1995). Wave-driven flow over shallow reefs. *Journal of Geophysical Research*, *100*(C2), 2639–2648. https://doi.org/10.1029/94JC02736

Taebi, S., Lowe, R. J., Pattiaratchi, C. B., Ivey, G. N., & Symonds, G. (2011). Modelling nearshore circulation in a fringing reef system: Ningaloo Reef, Australia. *Journal of Coastal Research*, *64*, 1200–1203. https://doi.org/10.2307/26482364

Takeshita, Y., Cyronak, T., Martz, T. R., Kindeberg, T., & Andersson, A. J. (2018). Coral reef carbonate chemistry variability at different functional scales. *Frontiers in Marine Science*, *5*, 362. https://doi.org/10.3389/fmars.2018.00175

Tilstra, A., van Hoytema, N., Cardini, U., Bednarz, V. N., Rix, L., Naumann, M. S., et al. (2018). Effects of water column mixing and stratification on planktonic primary production and dinitrogen fixation on a northern Red Sea coral reef. *Frontiers in Microbiology*, *9*, 2351. https://doi.org/10.3389/fmicb.2018.02351

Unsworth, R. K. F., Collier, C. J., Henderson, G. M., & McKenzie, L. J. (2012). Tropical seagrass meadows modify seawater carbon chemistry: Implications for coral reefs impacted by ocean acidification. *Environmental Research Letters*, *7*(2), 024026. https://doi.org/10.1088/1748-9326/7/2/024026

van Hooidonk, R., Maynard, J., Tamelander, J., Gove, J., Ahmadia, G., Raymundo, L., et al. (2016). Local-scale projections of coral reef futures and implications of the Paris Agreement. *Scientific Reports*, *6*(1), 39666. https://doi.org/10.1038/srep39666

van Hooidonk, R., Maynard, J. A., & Planes, S. (2013). Temporary refugia for coral reefs in a warming world. *Nature Climate Change*, *3*(5), 508–511. https://doi.org/10.1038/NCLIMATE1829

Venti, A., Kadko, D., Andersson, A. J., Langdon, C., & Bates, N. R. (2012). A multi-tracer model approach to estimate reef water residence times. *Limnology and Oceanography: Methods*, *10*(12), 1078–1095. https://doi.org/10.4319/lom.2012.10.1078

Vetter, O., Becker, J. M., Merrifield, M. A., Pequignet, A. C., Aucan, J., Boc, S. J., & Pollock, C. E. (2010). Wave setup over a Pacific Island fringing reef. *Journal of Geophysical Research*, *115*(12), C12066. https://doi.org/10.1029/2010JC006455

Wijgerde, T., Spijkers, P., Karruppannan, E., Verreth, J. A. J., & Osinga, R. (2012). Water flow affects zooplankton feeding by the scleractinian coral *Galaxea fascicularis* on a polyp and colony level. *Journal of Marine Biology*, *2012*, e854849-7. https://doi.org/10.1155/2012/854849

Winter, G., Castelle, B., Lowe, R. J., Hansen, J. E., & McCall, R. (2020). When is flow re-entrainment important for the flushing time in coastal reef systems? *Continental Shelf Research*, *206*(4), 104194. https://doi.org/10.1016/j.csr.2020.104194

Wyatt, A. S. J., Leichter, J. J., Toth, L. T., Miyajima, T., Aronson, R. B., & Nagata, T. (2020). Heat accumulation on coral reefs mitigated by internal waves. *Nature Geoscience*, *359*, 1–7. https://doi.org/10.1038/s41561-019-0486-4

Zhang, Z., Falter, J., Lowe, R., & Ivey, G. (2012). The combined influence of hydrodynamic forcing and calcification on the spatial distribution of alkalinity in a coral reef system. *Journal of Geophysical Research*, *117*(C4), 18. https://doi.org/10.1029/2011JC007603

Zhang, Z., Lowe, R., Falter, J., & Ivey, G. (2011). A numerical model of wave- and current-driven nutrient uptake by coral reef communities. *Ecological Modelling*, *222*(8), 1456–1470. https://doi.org/10.1016/j.ecolmodel.2011.01.014